

# Examining Tropical Cyclone Structure and Intensification with the FLIGHT+ Dataset from 1999 to 2012

JONATHAN MARTINEZ AND MICHAEL M. BELL

*Department of Atmospheric Science, Colorado State University, Fort Collins, Colorado*

JONATHAN L. VIGH

*National Center for Atmospheric Research, Boulder, Colorado*

ROBERT F. ROGERS

*Hurricane Research Division, NOAA/Atlantic Oceanographic and Meteorological Laboratory, Miami, Florida*

(Manuscript received 19 January 2017, in final form 28 July 2017)

## ABSTRACT

A comprehensive examination of tropical cyclone (TC) kinematic and thermodynamic structure in the Atlantic basin is created from the Extended Flight Level Dataset for Tropical Cyclones (FLIGHT+, version 1.1). In situ data collected at the 700-hPa flight level by NOAA WP-3D and USAF WC-130 aircraft from 1999 to 2012 are analyzed. A total of 233 azimuthal mean profiles comprising 1498 radial legs are stratified by TC intensity and 12-h intensity change. A matrix of composite structures is created for minor (category 1 and 2) and major (category 3 and above) hurricanes that are intensifying [intensity increase  $\geq 10$  kt  $(12\text{ h})^{-1}$ ], steady state [intensity change between  $\pm 5$  kt  $(12\text{ h})^{-1}$ ], and weakening [intensity decrease  $\leq -10$  kt  $(12\text{ h})^{-1}$ ]. Additional considerations to the impacts of age on TC structure are given as well. Axisymmetric radial composites reveal that intensifying TCs have statistically significant structural differences from TCs that are steady state or weakening, but that these differences also depend on the intensity of the TC. Intensifying TCs (both minor and major hurricanes) are characterized by steep tangential wind gradients radially inward of the radius of maximum tangential wind (RMW) that contribute to a ringlike structure of vorticity and inertial stability. Tangential wind structural differences are more pronounced in the eye of minor hurricanes compared to major hurricanes. Intensifying TCs are found to have higher inner- and outer-core moisture compared to steady-state and weakening TCs. Furthermore, intensifying major hurricanes possess drier eyes compared to steady-state and weakening major hurricanes.

## 1. Introduction

The structure of a tropical cyclone (TC) is influenced by both internal processes, such as convective bursts, eyewall replacement cycles, vortex Rossby waves, and upper-level outflow, as well as external processes and influences, such as environmental vertical wind shear, ocean surface temperatures and heat content, and synoptic-scale forcing. These physical processes are actively linked to the intensification of the TC and often manifest themselves as structural changes at various stages in the TC's life cycle. Understanding the relationship between TC structure and intensification is an

important aspect of our ability to forecast TC intensity change. DeMaria et al. (2014) demonstrated that although improvements in intensity forecast errors have not been as large as improvements in track forecast errors, they have improved over the past few decades especially at large forecast lead times (e.g., 48–120 h). However, the smallest improvements in TC intensity forecast errors occurred for the warning time frame (24–48 h). Further improvement of our understanding of the physical mechanisms involved in TC intensity change are required to minimize potential damage and fatalities caused by landfalling TCs in coastal communities.

Theoretical studies have demonstrated that one of the most important factors in determining the potential intensification of a TC is the intensity of the TC itself (Shapiro and Willoughby 1982; Vigh and Schubert

---

*Corresponding author:* Jonathan Martinez, jon.martinez@colostate.edu

2009). Higher intensities correspond to a reduction of the Rossby length that, in turn, increases the heating efficiency of the system. Furthermore, these studies demonstrated that the radial location of a heating source is a critical factor for TC intensification efficiency. Heating sources located radially inward of the radius of maximum tangential wind (RMW) in the region of high inertial stability are most efficient for vortex spinup (Schubert and Hack 1982). Smith and Montgomery (2016) argue that the axisymmetric radial wind flow response to the radial location of the heat source is more important than the heating efficiency, but agree that heating located radially inward of the RMW is more favorable for intensification than heating located radially outward of the RMW. The importance of the radial location of heating, and by implication the radial organization of convection, has been further confirmed by idealized numerical simulations (Pendergrass and Willoughby 2009).

Isolating the most important internal processes contributing to intensity change is difficult with observations due to limited sampling and the complexities of the real atmosphere, but features consistent with the above theoretical arguments have been observed in many TCs. Rogers et al. (2013) used a Doppler radar composite analysis to demonstrate that convective bursts (CBs) are preferentially located radially inward of the RMW in a region of high axisymmetric vorticity for intensifying TCs compared to radially outward of the RMW for steady-state TCs. The radar composites also indicated a distinct difference in the axisymmetric vorticity structure between intensifying and steady-state TCs. In the composite of intensifying storms, a ring structure exists with vorticity maximized away from the center but radially inward of the RMW. For the composite of steady-state storms, the vorticity structure is monopolar with a maximum near the center. These composite vorticity structures are similar to those found in an earlier flight level analysis by Kossin and Eastin (2001), in which intensifying TCs exhibit a vorticity ring structure, while steady-state TCs possess a monopolar vorticity structure. The vorticity ring structure satisfies the Rayleigh necessary condition for barotropic instability that can lead to a breakdown of the vorticity ring and concomitant formation of mesovortices, polygonal eyewalls, and radial mixing at the eye–eyewall interface. Radial mixing causes a rearrangement of the kinematic and thermodynamic fields such that the end state is a monopole (Schubert et al. 1999; Kossin and Eastin 2001).

The evolution of such instabilities in a nondivergent, barotropic framework have been shown to depend on the thickness of the vorticity ring and the ratio of vorticity in the eye compared to that in the eyewall (Kossin

and Schubert 2001; Hendricks et al. 2009). In the real atmosphere, axisymmetric eyewall heating drives the formation, strengthening, and thinning of a potential vorticity (PV) ring with time. Rozoff et al. (2009) demonstrated that “episodic” mixing events can occur in the presence of forcing, which acts to regenerate the vorticity ring after its breakdown. Mixing events resulting from barotropic instability act as a “transient intensification brake” during axisymmetric intensification, although the combined barotropic-convective instability that may be expected to occur in the real atmosphere can serve to intensify the vortex as the PV ring rolls up into convective mesovortices (Lee and Bell 2007; Rozoff et al. 2009; Hendricks et al. 2012, 2014).

It is challenging to discern the most important kinematic and thermodynamic structural features from observations due to asymmetric variability from different quadrants of the storm, temporal variability from consecutive aircraft penetrations and flights, and meteorological variability from the vast array of intensities, sizes, and environmental conditions. A composite approach allows for some reduction in this variability to identify common structural features across many TCs. One of the first studies to composite flight level data was Shea and Gray (1973), who used western Pacific aircraft reconnaissance data collected in TCs between 1957 and 1963. A component of their analysis stratified the data by a 24-h intensity change to address differences between TCs with deepening or filling central pressures. Although it was not explicitly stated in their discussion, the Shea and Gray (1973) composites revealed that deepening TCs have steeper radial gradients of tangential winds both radially inward and outward of the RMW compared to filling TCs (their Figs. 42 and 43). These differences in tangential wind gradients are consistent with the ring and monopolar vorticity structures found in intensifying and steady-state TCs, respectively, shown many years later by Kossin and Eastin (2001) and Rogers et al. (2013) using different datasets. A different compositing approach was used by Mallen et al. (2005), in which TCs were stratified by intensity instead of intensity change. Flight level composites using a similar Atlantic aircraft reconnaissance database as Kossin and Eastin (2001) revealed an increase of the tangential wind decay radially outward of the RMW with increasing intensity. Furthermore, Mallen et al. showed the existence of cyclonic vorticity in the outer-core region, which has important implications for vortex resiliency in the presence of vertical wind shear when compared to an idealized Rankine vortex.

In addition to intensity and intensity change, the structure of a TC can depend on its age. Kossin et al. (2007) demonstrated that the age of a TC could be used

as a predictor for its surface wind structure in a multiple regression model. In general, they found that the age (computed as the hours since tropical storm intensity was achieved) explains the most variance for the 64-kt critical wind radius ( $R_{64}$ ) and roughly the same amount of variance as the RMW for the 50-kt critical wind radius ( $R_{50}$ ). These results largely reflect the process by which the TC “broadens” its outer-core wind field with time. Generally speaking, heating concentrated in the eyewall updraft drives radial angular momentum convergence above the boundary layer, which leads to a spinup of the tangential circulation and thus an expansion of the vortex with time (Smith et al. 2009). Musgrave et al. (2012) further investigated the structural evolution of TCs with time as depicted on an integrated kinetic energy–maximum tangential wind diagram. The behavior of TCs in this phase space was shown to depend largely on the radial distribution of heating with respect to the RMW. Given that the radial distribution of heating evolves with time, the age of a TC can distinguish structural differences related to the physical processes that are largely forced by the radial location and influences of heating (e.g., secondary eyewalls and potential vorticity mixing). Differences in the outer-core heating can potentially lead to the formation of an “annular” structure as documented by Knaff et al. (2003), which would allow a TC to maintain its intensity for an extended period of time, or lead to the formation of a secondary eyewall that results in intensity fluctuations. The composite structure of eyewall replacement cycles was examined by Sitkowski et al. (2011), which demonstrated the distinct changes in the RMW and intensity resulting from the formation of a secondary eyewall.

These prior studies suggest that important structural features can be elucidated from the composite approach, but structural differences can be due to many different factors including both internal and external influences. Hendricks et al. (2010) suggested that TC intensification rates are mostly controlled by internal processes given a favorable preexisting environment. This study seeks to identify structural differences that are largely controlled by these internal processes rather than environmental influences. In contrast to the aforementioned approaches that separated composites based on a single parameter, the present study utilizes a more comprehensive approach through a multivariate stratification of TC structure by intensity, intensity change, age, and the presence of a secondary wind maximum. A multivariate stratification can aid in revealing new information regarding internal processes associated with intensity and structure change, but a large sample size is required to use this approach. We

employ the Extended Flight Level Dataset for Tropical Cyclones (FLIGHT+, version 1.1; Vigh et al. 2016) to examine the structure of North Atlantic TCs from 1999 to 2012. The large number of flight level profiles contained within the FLIGHT+ dataset allows for this multivariate analysis while retaining large enough sample sizes to provide statistically significant results. The results are broadly consistent with some previous studies, but reveal new insights into the differences between intensifying, steady-state, and weakening TCs at different stages of their life cycle. Section 2 will describe the methods involved in creating the various stratifications along with the description and processing of the data. Sections 3 and 4 will highlight the composite kinematic results and thermodynamic results, respectively. Section 5 will discuss the differences between the composite structures, and finally, conclusions and opportunities for future work will be presented in section 6.

## 2. Data and methods

### a. Description and stratification of best track data

Creation of the flight level composites requires first determining the intensity, intensity change, and age of the TC nearest to the time it was sampled by the aircraft. Determination of the age of the TC will be discussed later in section 2c. A further stratification to remove TCs with secondary wind maxima was conducted and will be discussed in section 5e. The TC intensity and 12-h intensity change are determined using the National Hurricane Center’s Best Track (BT) database for TCs in the North Atlantic basin from 1999 to 2012 (Jarvinen et al. 1984; McAdie et al. 2009; Landsea and Franklin 2013). The BT data points are recorded at standard synoptic times (every 6 h), as well as nonsynoptic times that are often included when a TC makes landfall or experiences any other significant changes (e.g., peaks in intensity). Given the complexities of structural change at landfall, these cases are removed from the analysis by removing BT data points with nonsynoptic reference times and times where a TC is deemed too close to land. Further details on the method to determine proximity to land are given in the next section. Cases of extratropical transition are also removed from the BT data because of structural changes resulting from baroclinic processes. These cases are removed by screening the BT data based on the status of the storm (e.g., tropical storm, hurricane, or extratropical), which is provided in the BT database.

The BT intensity ( $BT v_{max}$ ), defined as the maximum 1-min sustained wind speed at 10 m above the surface (for an open-ocean exposure) given in knots ( $1 \text{ kt} = 0.51 \text{ m s}^{-1}$ ), is used to characterize TC intensity and to compute the 12-h intensity change centered around the

time of a given BT data point. Testing using backward and forward time differencing showed little sensitivity in the resulting composite structures (Martinez 2016). A matrix is created that includes two bins for intensity and three bins for 12-h intensity change, giving a total of six possible bin permutations for the BT data points. Here we denote “minor” hurricanes as category 1 and 2 ( $64 \leq \text{BT } v_{\max} < 96 \text{ kt}$ ) and “major” hurricanes as category 3 and above ( $\text{BT } v_{\max} \geq 96 \text{ kt}$ ) according to the Saffir–Simpson hurricane wind scale used for TCs in the Atlantic and eastern North Pacific.

The centered 12-h intensity change bins are defined as intensifying [IN, intensity increase  $\geq 10 \text{ kt (12 h)}^{-1}$ ], steady state [SS, intensity change between  $\pm 5 \text{ kt (12 h)}^{-1}$  inclusive], and weakening [WK, intensity decrease  $\leq -10 \text{ kt (12 h)}^{-1}$ ]. The IN and SS bin thresholds are similar to those in Rogers et al. (2013) who instead used an intensity change calculated over 12 h that was then extrapolated to a 24-h intensity change. Several different binning strategies were tested, but the definitions used here provide the best stratification of a roughly equal number of samples into physically relevant and distinct bins. We note here that the parsing of the BT data restricts the analysis to hurricanes that were at least of category 1 intensity and purely tropical.

### *b. Description and processing of flight level data*

The structures of TCs are examined using in situ data from version 1.1 of the FLIGHT+ dataset (Vigh et al. 2016), a comprehensive database containing in situ data recorded at flight level by the National Oceanic and Atmospheric Administration (NOAA) WP-3D and U.S. Air Force (USAF) WC-130 aircraft during flight missions through TCs from 1999 to 2012.<sup>1</sup> The midpoint date and time of each flight mission in the database are rounded to the nearest synoptic time, and flight missions are then matched to the BT data points binned by intensity and intensity change, as described in the previous section. Aircraft reconnaissance missions into TCs are typically flown at either the 850- or 700-hPa pressure level, but the 850-hPa flight level is mostly used for developing systems at tropical storm strength or lower. Since these systems are excluded from the analysis, the 700-hPa pressure level is exclusively chosen due to the small number of flight missions at the 850-hPa level into TCs of at least category 1 intensity. Tests including an

intensity bin below minor hurricane strength at 700 hPa showed much higher variability than the stronger TCs due to both large structural differences at this intensity and the smaller sample size. Therefore, depressions and tropical storms are excluded from this study.

Corrections are applied to both temperature and dewpoint temperature prior to any thermodynamic computations to correct for instrument wetting using the method described by Zipser et al. (1981). Eastin et al. (2002) found that this method did not completely remove wetting errors, but did reduce the average errors found during instrument wetting events by 30%–50%, corresponding to average temperature, specific humidity, and equivalent potential temperature errors of 0.6 K,  $0.5 \text{ g kg}^{-1}$ , and 2.7 K, respectively. A more accurate temperature correction using an infrared radiometer (Barnes et al. 1991; Eastin et al. 2002) is not possible for USAF WC-130 data due to lack of instrumentation. Therefore, the simpler, more consistent correction is applied to the entire dataset.

The azimuthal mean structure of a TC for each flight mission is calculated by averaging all of its constituent radial legs at each radial point. Figure 1 illustrates an example flight path taken into Hurricane Katrina (2005) by the USAF WC-130 aircraft. Multiple radial penetrations were flown through the center of Katrina during this flight mission, with a total of 10 radial legs included in the analysis (Fig. 1b). Radial legs are defined as an inbound flight path toward the center or an outbound flight path away from the center of a TC. FLIGHT+ uses the Hurricane Research Division (HRD) spline interpolation of the Willoughby–Chelmon wind centers (Willoughby and Chelmon 1982) and, therefore, is tracking the actual storm-relative wind center (which tends to be a few kilometers right of track of the geometric center that is tracked by the National Hurricane Center). “Good” radial legs require the aircraft to pass through or within 25 km of the center of the TC and have a radial extent of at least 45 km; those that do not meet this requirement are not included in the analysis. Additionally, radial legs are investigated individually to remove erroneous data. This is accomplished by subjectively examining all profiles of tangential wind, temperature, and dewpoint temperature for each radial leg and manually removing any legs that contain suspect features in tangential wind, temperature, or dewpoint that may be a result of instrumentation errors. Examples of these errors include near zero winds for an entire radial leg, artificial (wavelike) fluctuations in dewpoint temperature, and temperature or dewpoint temperature values that are constant for the entire radial leg. After instrument wetting correction and subjective inspection of the data, a minimum of two good radial legs for a

<sup>1</sup> Version 1.1 of the FLIGHT+ dataset has been updated to include flight missions between 1997–98 and 2013–15, although exclusion of these years in this study is not expected to change the outcome of the results given the sufficiently large sample size used in this study.

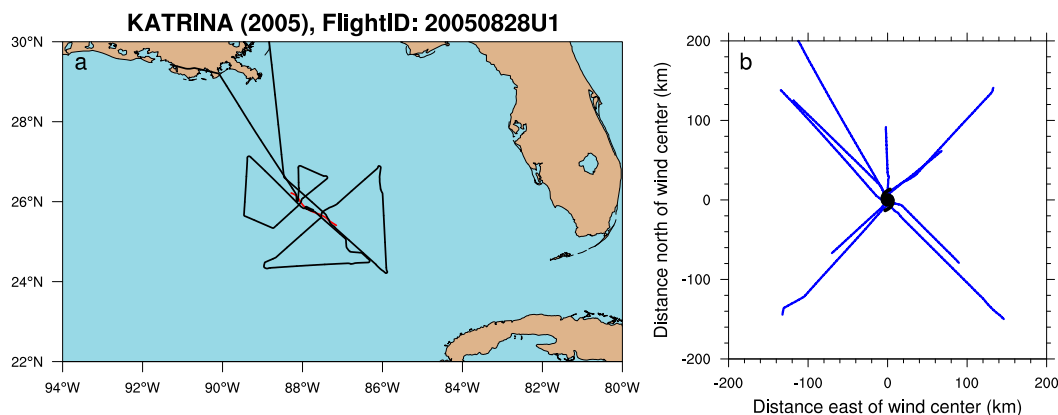


FIG. 1. (a) USAF WC-130 flight 20050828U1 through Hurricane Katrina as it traversed the Gulf of Mexico. The black lines denote the Earth-relative flight path of the aircraft and the wind centers determined by the Hurricane Research Division for the duration of the flight are shown in red. (b) The “good” radial legs that were flown are shown as a function of the storm-relative distance to the storm center, denoted by the hurricane symbol.

given flight mission are required for the calculation of the azimuthal mean and inclusion in the composite analysis. Continuing with the example flight mission through Hurricane Katrina, Fig. 2a illustrates the azimuthal averaging for the 10 radial legs used in the analysis.

The azimuthal mean structures are then smoothed using a one-dimensional 10-km Lanczos filter to remove small-scale transient features (Duchon 1979). Figure 2b demonstrates the ability of the filter to remove small-scale features yet retain the overall mesoscale shape of the azimuthal mean structure. The smoothing is also important for removing noise in calculated quantities that involve radial derivatives. After the smoothed azimuthal mean structures are computed, the data are screened for possible land interactions. The distance-to-land parameter provided by the Statistical Hurricane

Intensity Prediction Scheme (SHIPS; DeMaria et al. 2005) database is used to determine the distance between the center of the TC and the nearest major landmass. The data are restricted to the cases where the azimuthal mean RMW is greater than 20 km from the nearest landmass at any point during the 12-h intensity change window.

The final processing step for each azimuthal mean structure is to normalize the radius coordinate by the RMW. Normalization of the radial coordinate has been used in previous studies (Shea and Gray 1973; Mallen et al. 2005; Rogers et al. 2013) for the creation of composites of TCs with varying size. The normalization establishes a common reference point where the RMW occurs at a normalized radius of unity for each azimuthal mean, yet retains the overall shape of the azimuthal mean structure. Figure 2c shows the smoothed, normalized

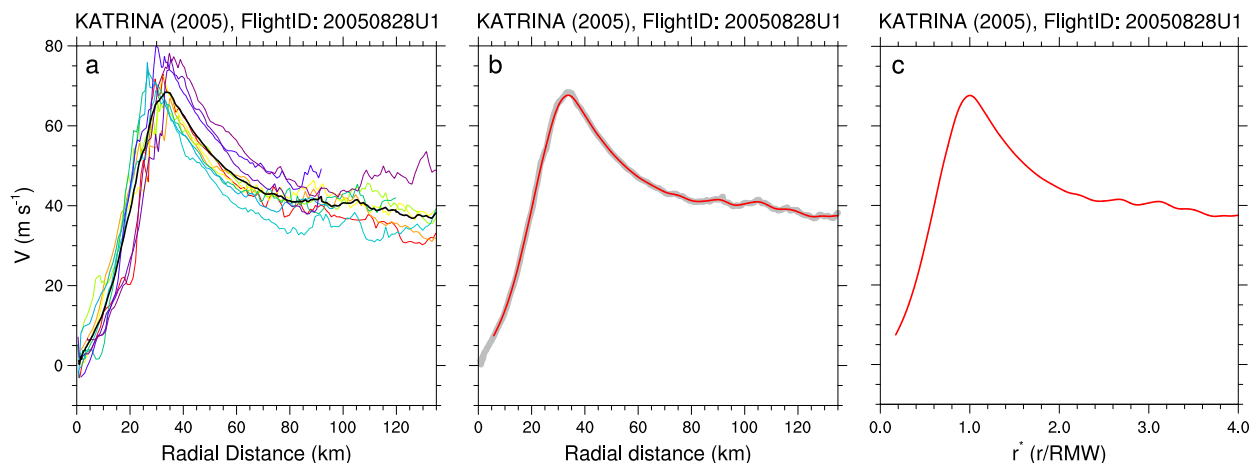


FIG. 2. (a) Storm-relative tangential wind velocity plotted as a function of radial distance for each of the good radial legs (denoted by different colors) and overlaid by the azimuthal mean (black) for flight 20050828U1 through Hurricane Katrina. (b) The azimuthal mean (gray) overlaid by the smoothed azimuthal mean (red). (c) The smoothed azimuthal mean profile plotted as a function of  $r^*$ .

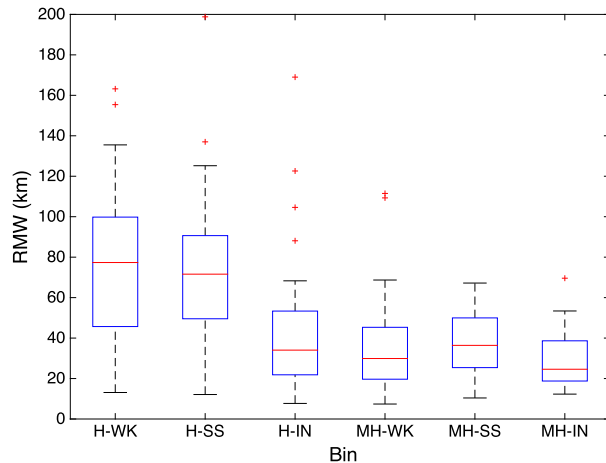


FIG. 3. Box-and-whisker plots for the RMW sizes (km) in each bin. The labels on the abscissa represent the intensity, denoted by the first letter (“H” for minor hurricane and “MH” for major hurricane) followed by the intensity change bin [weakening (WK), steady state (SS), intensifying (IN)]. The red line denotes the median RMW size while the upper and lower edges of the box represent the upper ( $q_{0.75}$ ) and lower ( $q_{0.25}$ ) quartiles, respectively. Whiskers extend to  $q_{0.75} + \text{IQR}$  and  $q_{0.25} - \text{IQR}$ , where IQR represents the interquartile range ( $q_{0.75} - q_{0.25}$ ). Outliers are defined outside of the range covered by the whiskers and denoted by red crosses.

azimuthal mean for the same flight mission through Hurricane Katrina to be used in its respective composite. The profile is identical to that seen in Fig. 2b, but with a different abscissa.

As mentioned by Shea and Gray, the normalization by RMW places an emphasis on the inner-core region of TCs by separating the dynamically different regions radially inward and outward of the RMW. However, this method also contains some inherent drawbacks. For example, it obscures any information relating to the size of the TC. Additionally, the azimuthal mean RMW is often influenced by the asymmetric distribution of convection. Furthermore, if there is large variability in the size of the RMWs, then normalization of the radial coordinate can distort the shape of the profiles and will ultimately result in averaging across different physical radii when computing the composite means. Figure 3 provides insight to the degree of variability in RMW sizes for the different bins used to stratify the dataset. The variability is largest for the WK and SS minor hurricanes, and has a similar magnitude for IN minor hurricanes and all major hurricanes. Despite this variability and the aforementioned trade-offs, the normalization is believed to be a viable method that provides insight into the composite structure of a TC in a dynamically relevant way.

Henceforth, the quality-controlled, smoothed, and radially normalized azimuthal means will be referred to as the azimuthal mean profiles and the normalized

radius coordinate will be denoted by  $r^*$ . After the above-described screening and processing steps, a total of 233 azimuthal mean profiles remained, comprising 1498 radial legs through TCs from 1999 to 2012. Table 1 details the specific number of flight missions into each TC included in the analysis along with the corresponding flight IDs and number of good radial legs retained for each flight mission. These constitute the data analyzed in this study. Table 2 highlights the number of azimuthal mean profiles in the matrix of each intensity and intensity change bin. The stratification results in a range of 22–48 azimuthal mean profiles for each bin, with an average of 39 per bin. Figure 4 highlights the number of azimuthal mean profiles included in the composite means stratified by intensity and intensity change as a function of the normalized radius  $r^*$ , demonstrating that the composite-mean sample sizes for a given  $r^*$  are variable.

### c. Stratification by TC age

To characterize the TC structural features by stage of the TC life cycle, the azimuthal mean profiles are further stratified according to the age of the TC at the midpoint time of each flight mission. The TC lifetime is computed by subtracting the time between the last reported BT data point (excluding extratropical transition) and the first reported BT data point that occurs when tropical depression status is achieved (i.e., genesis as defined herein). This method differs slightly from that used by Kossin et al. (2007) who instead used the time since tropical storm formation, although we do not expect our results to be sensitive to this choice. The “flight age” of a TC is computed by subtracting genesis from the midpoint time of a flight mission into that TC, and then normalizing by the TC lifetime. This method is used to provide insight to when the flight mission (and its corresponding azimuthal mean profile) occurs relative to the specific life cycle of that TC. For simplicity, the azimuthal mean profiles are then defined as “early” stage if their normalized age is below the bin-average-normalized flight age for their respective bin, and “late” stage if their age is above the bin average. Using a bin-specific threshold allows for an approximately equal distribution of azimuthal mean profiles into the subsequent 12 bins stratified by TC intensity, 12-h intensity change, and age. Tests using a 0.5 normalized age as a threshold produce an uneven distribution that is less conducive for statistically significant comparison between the bins. Table 3 highlights the number of azimuthal mean profiles (sample size) in each of the 12 bins resulting from this stratification. While this additional stratification reduces the number of azimuthal mean profiles in each bin, some statistically significant and physically relevant results are still obtained and will be discussed in section 5. Furthermore, Table 4 provides

information on both the composite-mean true age (in days) and normalized age for each of the 12 bins. Figure 5 highlights the number of azimuthal mean profiles included in the composite means additionally stratified by age as a function of the normalized radius  $r^*$ .

### 3. Axisymmetric kinematic composite-mean structures

#### a. Tangential wind velocity

The storm-relative axisymmetric tangential wind velocity composite means ( $V_T$ ) for each bin are provided in Fig. 6. Radial locations where two or more composite means had statistically significant differences at the 5% level using a two-tailed Wilcoxon–Mann–Whitney (WMW) rank-sum test appear thicker on the respective composite-mean curves. To simplify the discussion of the results that follows, we arbitrarily define the following radial regions within the TCs:

- the eye is defined to be radially inward of  $r^* = 0.6$ ,
- the inner core (including the eyewall) is defined to be between  $r^* = 0.6$  and 2, and
- the outer core lies radially outward of  $r^* = 2$ .

The minor hurricane  $V_T$  profiles exhibit the greatest differences in the eye, where IN minor hurricanes have the steepest increase of  $V_T$  followed by SS and then WK minor hurricanes. The magnitude of the statistically significant  $V_T$  differences in the eye of minor hurricanes is on the order of  $2\text{--}6\text{ m s}^{-1}$ , while differences in the inner- and outer-core regions are minimal. Contrary to the minor hurricanes, major hurricanes do not possess any notable significant differences in  $V_T$  radially inward of the RMW. Major hurricanes exhibit more differences in the outer-core region, where WK major hurricanes possess the slowest decay of  $V_T$  followed by SS and then IN major hurricanes. Statistically significant differences in outer-core  $V_T$  are on the order of  $2\text{--}4\text{ m s}^{-1}$ . We note that no statistically significant differences are found between the composite-mean structures of radial wind (not shown).

#### b. Vertical vorticity

Axisymmetric vertical vorticity is given by  $\zeta = \bar{V}/r + \partial\bar{V}/\partial r$ , where  $\bar{V}$  represents the smoothed azimuthal mean storm-relative tangential wind velocity and  $r$  is the radial distance. Figure 7 shows the axisymmetric vertical vorticity composite means for each bin. In general, IN TCs (minor and major hurricanes) possess a ringlike structure of vorticity with vorticity maximized radially inward of the RMW. The IN minor hurricane vorticity is significantly larger than both SS and WK minor hurricane vorticity in the eye and inner-core region, with a peak difference of  $\sim 15 \times 10^{-4}\text{ s}^{-1}$ . Both IN and WK

major hurricanes possess a vorticity ring structure in the eye, while SS major hurricanes possess a flatter vorticity profile indicative of a more stable regime. Statistically significant differences in eye vorticity for IN major hurricanes compared to SS major hurricanes ranges between approximately  $10$  and  $20 \times 10^{-4}\text{ s}^{-1}$ . Overall, major hurricanes possess nearly twice the vorticity in the eye compared to minor hurricanes for each respective intensity change bin. In the outer core, IN minor hurricanes possess larger vorticity compared to SS and WK minor hurricanes. In contrast, WK major hurricanes have larger vorticity in the outer core compared to IN or SS major hurricanes, although this difference will be shown in section 5e to be primarily due to secondary eyewalls.

#### c. Inertial stability

Axisymmetric inertial stability is given by  $I^2 = (f + \zeta)(f + \bar{V}/r)$ , where  $f$  is the Coriolis parameter evaluated at the RMW for a given azimuthal mean profile. The inertial stability composite means are shown in Fig. 8. It is evident from these results that the inertial stability profiles in all minor and major hurricanes are quite similar to their constituent vorticity profiles. A ringlike structure of inertial stability exists in the eye of IN minor and major hurricanes, as well as WK major hurricanes. Furthermore, IN minor hurricanes possess higher inner- and outer-core inertial stability compared to SS and WK minor hurricanes, although the magnitude of these differences are small compared to those found in the eye. Specifically, IN minor hurricanes possess anywhere between  $2$  and  $6 \times 10^{-6}\text{ s}^{-2}$  more inertial stability in the eye compared to WK or SS minor hurricanes. The differences diminish rapidly from the inner to the outer core, decreasing from a maximum difference of  $\sim 6 \times 10^{-6}\text{ s}^{-2}$  near  $r^* = 0.8$  to less than  $1 \times 10^{-6}\text{ s}^{-2}$ . The IN major hurricanes possess significantly higher inertial stability in the eye and inner core compared to SS major hurricanes, with statistically significant differences ranging between  $10$  and  $16 \times 10^{-6}\text{ s}^{-2}$  in the eye and  $1$  and  $15 \times 10^{-6}\text{ s}^{-2}$  in the inner core. Overall, major hurricanes possess anywhere between  $2$  and  $8$  times more inertial stability radially inward of the RMW compared to minor hurricanes for each respective intensity change bin, demonstrating that the eye and inner-core region of major hurricanes are much more inertially resistant compared to minor hurricanes.

#### d. Absolute angular momentum

The axisymmetric absolute angular momentum is given by  $M = r\bar{V} + fr^2/2$ . The results for the  $M$  composite-mean profiles present large variability within each bin due its strong radial dependence. To adjust for this variability,  $M$  was normalized by its value at the RMW prior to computing the composite means to

TABLE 1. List of each tropical cyclone included in the analysis. The corresponding number of flight missions, flight IDs, and number of radial legs that comprised each azimuthal mean profile in the analysis are included for reference.

Cyclone	Year	Profiles	Flight ID (No. of radial legs)
Bret	1999	3	0821U2 (5), 0822U1 (9), 0822U2 (10)
Dennis	1999	8	0827U4 (3), 0827U5 (5), 0828U1 (10), 0828U2 (7), 0828U3 (8), 0829U1 (6), 0829U2 (8), 0831U1 (3)
Floyd	1999	11	0910U2 (7), 0911U1 (8), 0911U2 (8), 0912U1 (8), 0912U2 (10), 0913U1 (7), 0914U1(6), 0914U2 (8), 0914U3 (7), 0915U1 (6), 0915U2 (5)
Gert	1999	6	0916U1 (4), 0916U2 (4), 0917U1 (2), 0920U2 (4), 0921U2 (4), 0921U3 (2)
Lenny	1999	8	1116I1 (3), 1116U2 (5), 1117U1 (6), 1117U2 (3), 1117U3 (8), 1118U1 (5), 1118U2 (6), 1119U1 (4)
Debby	2000	1	0822U1 (10)
Keith	2000	1	1001U1 (5)
Erin	2001	2	0909_AF980_0706A (7), 0909_AF985_0806A (7)
Humberto	2001	2	0923_AF861_0410A (3), 0924_AF977_0610A (4)
Iris	2001	4	1007_AF966_0511A (7), 1007h1 (7), 1008_AF967_0711A (8), 1008_AF966_0811A (11)
Michelle	2001	4	1103_AF966_1015A (6), 1103_AF861_1115A (4), 1103H1 (2), 1104H1 (10)
Isidore	2002	3	0920U1 (6), 0921U1 (8), 0922U2 (6)
Lili	2002	3	0930U2 (7), 1002U1 (10), 1003U1 (9)
Claudette	2003	1	0710U2 (5)
Fabian	2003	7	0902U1 (4), 0903U1 (4), 0903U2 (4), 0904U1 (2), 0904U3 (4), 0905U1 (8), 0905U3 (8)
Isabel	2003	11	0912U1 (4), 0913U1 (4), 0913U2 (3), 0914U1 (3), 0914U2 (3), 0915U1 (4), 0916U1 (3), 0916U2 (7), 0917U1 (7), 0917U2 (5), 0917U3 (8)
Alex	2004	1	0803u2 (4)
Charley	2004	2	0812u2 (9), 0812u3 (9)
Frances	2004	14	0830u1 (7), 0830I1 (4), 0831u1 (7), 0831u2 (7), 0901u1 (7), 0901u2 (9), 0902u1 (9), 0902u2 (5), 0902u3 (8), 0903u1 (4), 0903u2 (7), 0903u3 (9), 0904u1 (7), 0904u2 (6)
Ivan	2004	17	0906u2 (7), 0907u1 (7), 0907u2 (9), 0908u1 (7), 0908u2 (7), 0909u1 (9), 0909u2 (6), 0909I1 (2), 0910u1 (5), 0910u2 (8), 0911u2 (10), 0912u1 (7), 0912u2 (6), 0913u1 (5), 0914u1 (10), 0915u2 (4), 0915u3 (6)
Jeanne	2004	4	0924u2 (8), 0924u3 (6), 0925I1 (8), 0925u1 (8)
Dennis	2005	5	0707U1 (6), 0707U2 (11), 0708H1 (5), 0709U2 (9), 0709U3 (11)
Emily	2005	8	0714U1 (7), 0714U2 (6), 0715U1 (10), 0716U1 (8), 0717U1 (8), 0718U1 (10), 0719U1 (8), 0719U2 (10)
Katrina	2005	6	0826U1 (10), 0827I1 (3), 0827U1 (10), 0827U3 (8), 0828I1 (10), 0828U1 (10)
Nate	2005	1	0908U1 (4)
Ophelia	2005	2	0910U1 (6), 0910U2 (10)
Philippe	2005	1	0918U3 (6)
Rita	2005	7	0920U1 (6), 0921U1 (8), 0922U1 (8), 0922I1 (10), 0922U2 (7), 0923U1 (8), 0923I1 (10)
Wilma	2005	7	1019U2 (3), 1020U1 (8), 1020H1 (8), 1020h1 (2), 1021U1 (8), 1023U2 (10), 1023U3 (11)
Beta	2005	1	1029U1 (4)
Ernesto	2006	1	0827U1 (5)
Florence	2006	2	0910U2 (10), 0911U1 (8)
Dean	2007	6	0817U1 (8), 0817U2 (6), 0818U1 (10), 0818U2 (11), 0819U2 (7), 0820U2 (10)
Felix	2007	4	0902U1 (5), 0902U2 (4), 0903U1 (4), 0903U3 (6)
Noel	2007	1	1101U2 (4)
Bertha	2008	2	0711U1 (2), 0712U1 (4)
Gustav	2008	2	0826U1 (8), 0830U1 (11)
Ike	2008	10	0905U3 (4), 0906U1 (4), 0906U2 (6), 0907U1 (8), 0910U2 (7), 0910U1 (9), 0911U1 (8), 0911U2 (8), 0912U1 (10), 0912U2 (8)
Omar	2008	2	1015U1 (7), 1015U2 (6)
Paloma	2008	2	1107U2 (8), 1108U1 (6)
Bill	2009	8	0818U1 (2), 0819U1 (2), 0820U1 (4), 0820U2 (4), 0821U1 (4), 0821U2 (3), 0822U1 (4), 0822U2 (4)
Ida	2009	3	1108U1 (4), 1108U2 (8), 1109U1 (8)
Danielle	2010	2	0827U1 (3), 0828U1 (4)
Earl	2010	9	0829U2 (6), 0830U1 (6), 0830U2 (9), 0831U1 (5), 0901U1 (4), 0902U1 (7), 0902U2 (8), 0902U3 (8), 0903U2 (6)
Igor	2010	6	0916U2 (4), 0917U2 (4), 0918U1 (2), 0918U2 (4), 0919U1 (4), 0919U2 (8)
Karl	2010	1	0916U4 (4)

TABLE 1. (Continued)

Cyclone	Year	Profiles	Flight ID (No. of radial legs)
Paula	2010	2	1013U1 (5), 1013U2 (9)
Irene	2011	9	0823U2 (8), 0823U3 (6), 0824U1 (5), 0824U2 (8), 0825U1 (8), 0825U2 (6), 0826U1 (8), 0826U2 (8), 0826U3 (7)
Katia	2011	1	0906U1(2)
Rina	2011	4	1025U2 (4), 1026U1 (5), 1026U2 (5), 1027U1 (3)
Rafael	2012	1	1016U1 (7)
Sandy	2012	4	1026U1 (6), 1027U3 (7), 1028U1 (7), 1028U2 (8)

yield a nondimensional absolute angular momentum  $M^*$ . The  $M^*$  profiles were then composited for each bin and these results are presented in Fig. 9. These results are generally consistent with what we would expect given the  $V_T$  composite means in Fig. 6. The IN minor hurricanes exhibit the lowest  $M^*$  radially inward of the eye, followed by SS and then WK minor hurricanes. Major hurricanes exhibit slightly less variability in the eye although the differences are statistically significant at the 5% level. Overall, IN TCs (minor and major hurricanes) are characteristic of the lowest  $M^*$  in the outer-core region, which also holds true for dimensional  $M$  as a function of  $r^*$  (not shown).

#### 4. Thermodynamic composite-mean structures

##### a. Temperature

The results for the composite-mean temperature structures are shown in Fig. 10 and in general show small differences for both minor and major hurricanes. The IN minor hurricanes have slightly warmer eyes at the 700-hPa flight level compared to SS or WK minor hurricanes. The magnitude of the statistically significant differences between IN and WK minor hurricanes in the eye are on the order of 1 K. On the other hand, WK major hurricanes possess warmer temperatures in the inner- and outer-core regions compared to IN and SS major hurricanes, with statistically significant differences on the order of 1 K as well.

##### b. Specific and relative humidity

Figures 11 and 12 highlight the composite-mean structures of specific and relative humidity (RH), respectively. The IN minor hurricanes are found to possess higher specific humidity at all  $r^*$  compared to SS and WK minor hurricanes, with statistically significant differences ranging between 0.5 and 2 g kg<sup>-1</sup>. Although large differences in specific humidity are not found in the inner- and outer-core regions of major hurricanes, the composite-mean structures of RH demonstrate an interesting result: IN TCs (minor and major hurricanes) possess higher inner- and outer-core RH compared to SS or WK TCs, significant at the 5% level.

Statistically significant differences in the inner- and outer-core RH range between 3%–10% and 3%–6% for minor hurricanes and major hurricanes, respectively. The IN major hurricanes are also found to have drier eyes compared to SS or WK major hurricanes as shown in both Figs. 11b and 12b. Specifically, IN major hurricanes possess between 0.5–1.5 g kg<sup>-1</sup> lower specific humidity and ~4%–10% lower RH in the eye region compared to SS major hurricanes, statistically significant at the 5% level.

##### c. Equivalent potential temperature

Calculation of equivalent potential temperature  $\theta_e$  follows the empirical formulas derived by Bolton (1980), and the composite-mean structures are shown in Fig. 13. The higher temperature and specific humidity for IN minor hurricanes at nearly all  $r^*$  contributes to higher  $\theta_e$  when compared to the SS and WK minor hurricanes. Statistically significant differences between IN and SS minor hurricanes range from 1 to 2 K while statistically significant differences between IN and WK minor hurricanes are on the order of ~3 K. In contrast to the minor hurricanes, there are minimal differences among the major hurricane  $\theta_e$  composite means. The WK major hurricanes generally have the highest  $\theta_e$  compared to SS and IN major hurricanes, but these results are generally not statistically significant aside from WK major hurricanes possessing ~4 K higher  $\theta_e$  than SS major hurricanes between  $r^* = 3$  and 4.

## 5. Discussion

##### a. Gradients of tangential wind

The differences in the  $V_T$  gradients radially inward and outward of the RMW documented here are

TABLE 2. Summary of the number of flights that are matched to a BT fit for each intensity and centered 12-h intensity change bin. The thresholds for each bin according to intensity and intensity change are described in section 2.

	Minor hurricane	Major hurricane
IN	44	41
SS	48	47
WK	22	31

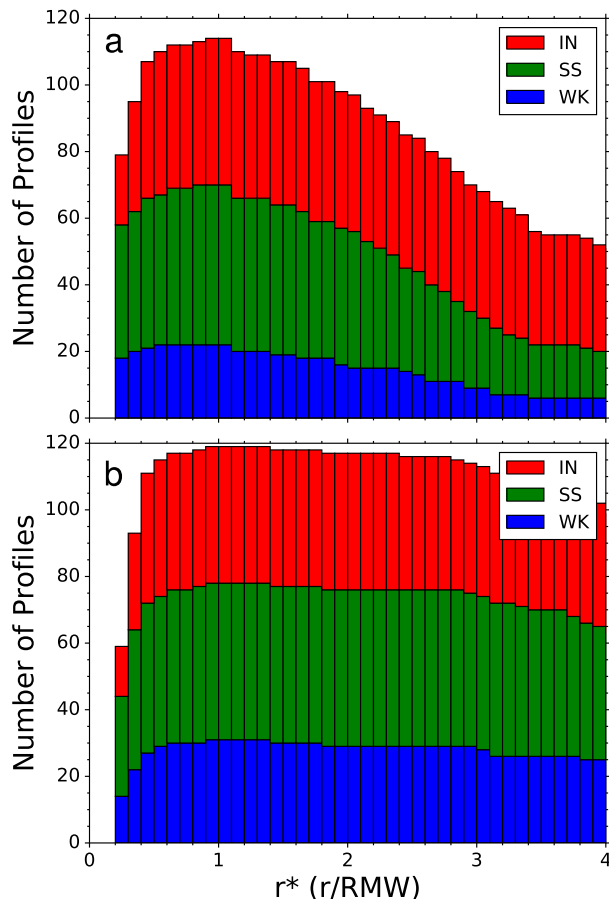


FIG. 4. Cumulative bar graphs representing the number of azimuthal mean profiles included in the respective composite means at each normalized radial point for (a) minor hurricanes and (b) major hurricanes. Intensifying (IN) TCs are denoted in red, steady-state (SS) TCs are denoted in green, and weakening (WK) TCs are denoted in blue. We note that sample sizes are shown every  $0.1 \times r^*$  for plotting purposes but data on the normalized radial grid are originally presented at a resolution of  $0.01 \times r^*$ .

consistent with those presented in previous studies (Kossin and Eastin 2001; Shea and Gray 1973; Willoughby 1990). The results presented here confirm that both the presence (or absence) of strong convection located radially inward of the RMW and radial mixing at the eye–eyewall interface are significant influences in the observed  $V_T$  gradient differences between WK, SS, and IN TCs. The steep  $V_T$  gradients and vorticity ring structure of IN minor and major hurricanes supports the presence of a strong “convective ring” as observed and discussed by Willoughby (1990). Stronger  $V_T$  evident in the eye of WK and SS minor hurricanes (Fig. 6) supports the transition toward solid-body rotation discussed by Kossin and Eastin (2001) after the breakdown of a vorticity ring. This is further supported by higher  $M^*$  in the eye of SS and WK minor hurricanes (Fig. 9).

TABLE 3. Summary of the number of flights that are matched to a BT fix for each intensity, centered 12-h intensity change, and age bin. The thresholds for each bin according to intensity, intensity change, and age are described in section 2.

	Minor hurricane		Major hurricane	
	Early	Late	Early	Late
IN	25	19	21	20
SS	19	29	24	23
WK	9	13	17	14

Compared with major hurricanes, minor hurricanes possess much larger differences between the  $V_T$  and  $M^*$  profiles in the eye region. It is interesting to note that the  $V_T$  differences are greatest radially inward of the RMW for minor hurricanes and radially outward of the RMW for major hurricanes. Thus, compared to major hurricanes, the  $V_T$  structure in the eye of minor hurricanes may be more demonstrative of changes caused by radial mixing near the eye and eyewall.

#### b. Vorticity ring structure and outer-core vorticity

Both IN minor and major hurricanes are found to possess a vorticity ring structure, suggesting that a vorticity ring, likely associated with the presence of strong convection located radially inward of the RMW, is an inherent feature of IN TCs. Rogers et al. (2013) and Rogers et al. (2015) demonstrated that for an IN TC, convective bursts (CBs) were primarily located radially inward of the RMW, collocated with high axisymmetric vertical vorticity, which would maximize the efficiency of heating produced by the CBs (Vigh and Schubert 2009). Although the flight level data utilized in this study precludes the observation of CBs, the similarities of our results with those presented by Rogers et al. suggest that CBs may be contributing to the vorticity ring through vortex tube stretching enhanced by low-level convergence in that region. It should be noted that CBs typically have time scales on the order of 1–3 h (Rogers 2010) so it is difficult to fully attribute the observed

TABLE 4. Composite-mean flight age and normalized flight age for each intensity and centered 12-h intensity change bin. Standard deviations are given in parentheses. See section 2c for a description on how the normalized flight age was computed.

Bin	Age (days)	Normalized age
Minor hurricanes		
IN	4.74 (2.69)	0.49 (0.22)
SS	6.78 (3.19)	0.64 (0.18)
WK	7.42 (2.72)	0.67 (0.18)
Major hurricanes		
IN	5.37 (2.15)	0.49 (0.16)
SS	6.70 (2.15)	0.56 (0.13)
WK	6.81 (2.44)	0.60 (0.14)

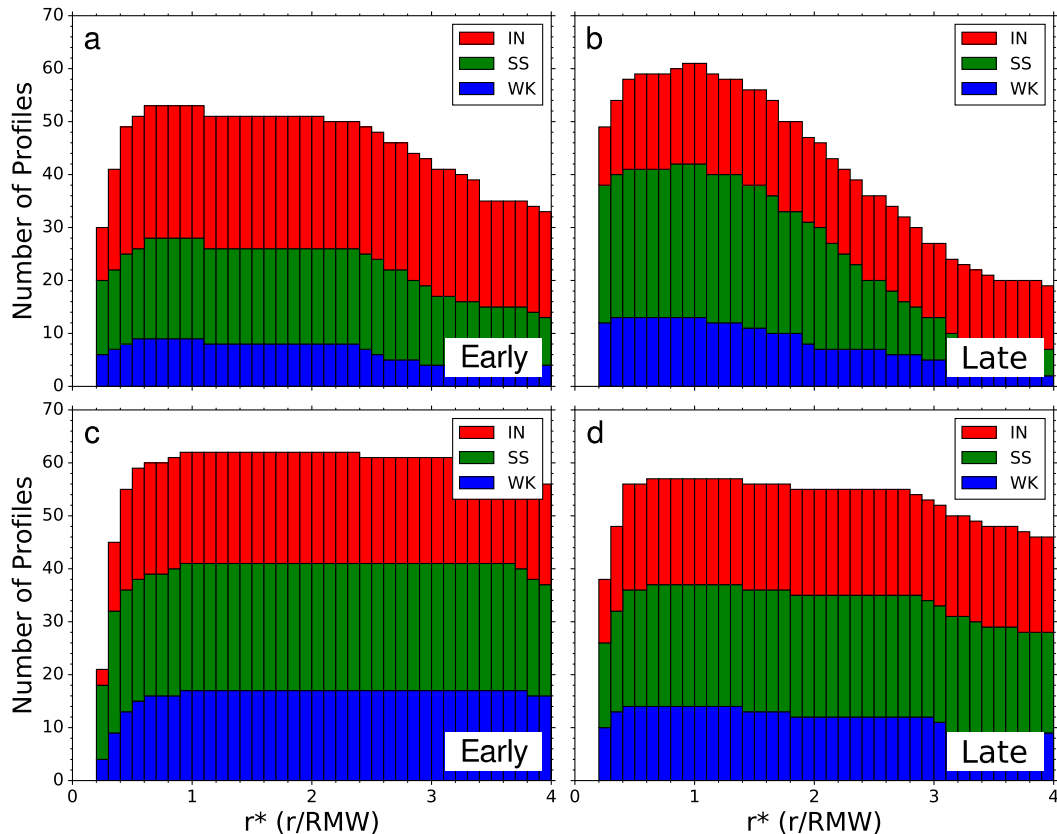


FIG. 5. As in Fig. 4, but for (a) early stage minor hurricanes, (b) late stage minor hurricanes, (c) early stage major hurricanes, and (d) late stage major hurricanes.

features in azimuthal mean structures, which can have time scales on the order of 6 h or more, directly to individual CBs. Additional averaging carried out to create the composite-mean structures would further smooth out these effects. However, the results demonstrate that intense convection located radially inward of the RMW is likely present for IN TCs given that the enhanced vorticity produced by CBs can project on to the azimuthal mean. In the case of WK major hurricanes, the vorticity ring may be formed through similar processes prior to the system reaching its weakening state and its amplitude is expected to decrease if the system continues to weaken. In the case of the monotonically decreasing vorticity structure that is observed in SS TCs and WK minor hurricanes, radial mixing at the eye-eyewall interface can rearrange the vorticity in a manner consistent with that proposed by Schubert et al. (1999) and observed in regime 2 (i.e., post-peak intensity) TCs by Kossin and Eastin (2001).

The WK major hurricanes possess slightly higher outer-core vorticity and inertial stability compared to SS and IN major hurricanes. In contrast, outer-core vorticity and inertial stability for IN minor hurricanes are

highest when compared to SS or WK minor hurricanes. The vorticity results for minor hurricanes contrast those presented by Rogers et al. (2013) who found higher outer-core vorticity for SS TCs compared to IN TCs. Furthermore, SS major hurricanes are found to have no statistically significant differences in outer-core vorticity and inertial stability when compared to IN major hurricanes, another result that contrasts those presented by Rogers et al. (2013). Discrepancies between the results presented in this study and those presented by Rogers et al. (2013) may have arisen from the different sample sizes, the different methods by which vorticity was calculated,<sup>2</sup> different stratification methods (e.g., this study

<sup>2</sup>Rogers et al. (2013) computed the vertical vorticity for each radial pass from Doppler-derived winds on a Cartesian grid, converted to cylindrical coordinates, azimuthally averaged, and then created the composite means. In this study, axisymmetric vertical vorticity is calculated in cylindrical coordinates from the smoothed azimuthal mean storm-relative tangential wind velocity ( $\bar{V}$ ) profiles and then the composite-mean vorticity is computed for each bin. Therefore, the spatial gradients resolved by the two calculations are different.

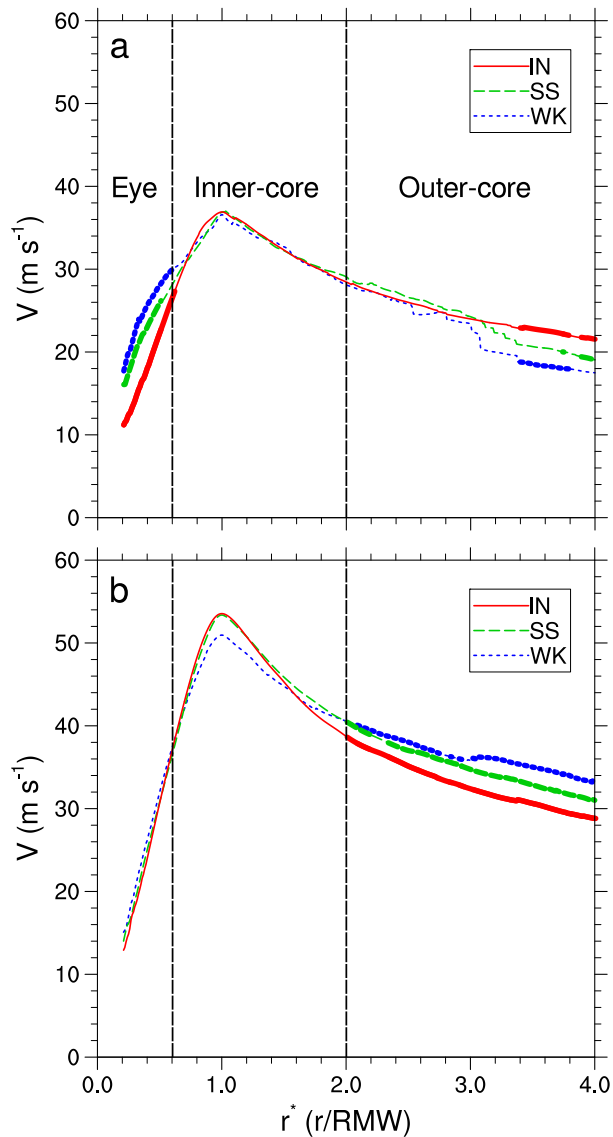


FIG. 6. Storm-relative axisymmetric tangential wind velocity composite means for (a) minor hurricanes and (b) major hurricanes. Intensifying (IN) TCs are denoted in solid red, steady-state (SS) TCs are denoted in dashed green, and weakening (WK) TCs are denoted in dotted blue. Radial locations where two composite means are significantly different at the 5% level appear thicker on the respective composite-mean curves. The vertical dashed lines correspond to the radial regions defined in section 3a.

stratifies by intensity), and the differences in the vertical levels available from Doppler radar versus the single pressure level examined here. Broadly speaking, the inner- and outer-core vorticity structure for all minor and major hurricanes demonstrate the presence of cyclonic vorticity as documented by [Mallen et al. \(2005\)](#), but that statistically significant differences in the magnitude of the outer-core vorticity among the different intensity change bins are mostly present for only minor hurricanes. We note that the

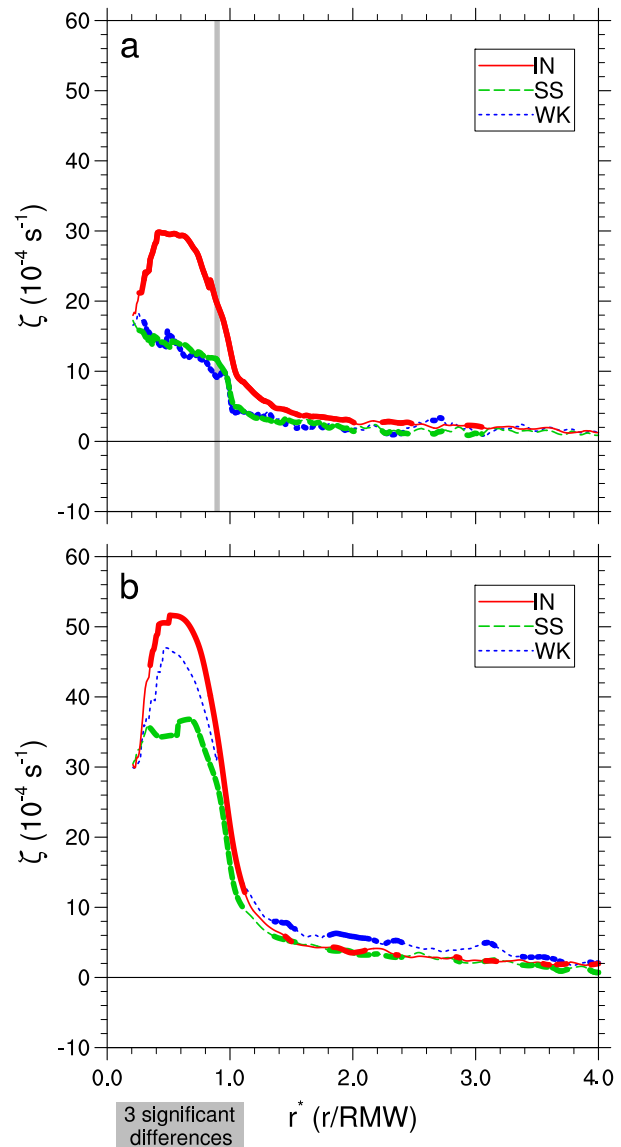


FIG. 7. As in Fig. 6, but for axisymmetric vertical vorticity. In this figure and the following, radial locations where all composite means are significantly different at the 5% level are shaded in gray.

larger values of outer-core vorticity associated with WK major hurricanes (Fig. 7b) are reduced when secondary eyewall cases are removed from the composite, which will be further discussed in section 5e.

Combining the results observed for  $V_T$  and vorticity when further stratifying by TC age (Figs. 14 and 15) highlights a significant change in the  $V_T$  and vorticity structure for WK major hurricanes. At early stages, WK major hurricanes possess a strong vorticity ring structure with a composite-mean peak vorticity value greater than that observed for IN major hurricanes. By the later

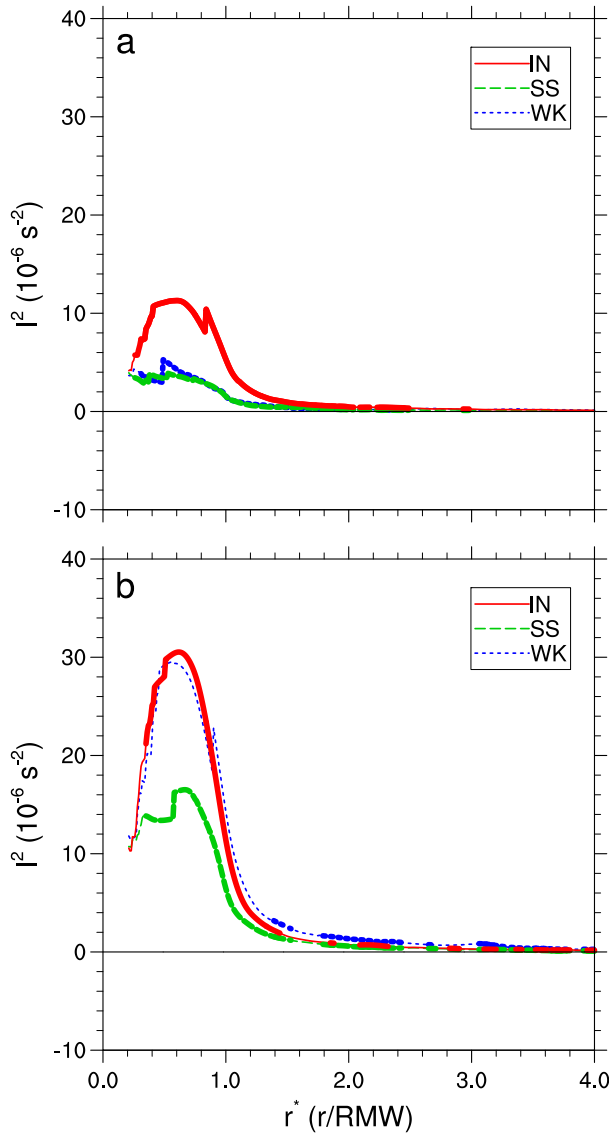


FIG. 8. As in Fig. 6, but for axisymmetric inertial stability.

stages, the vorticity ring completely vanishes and WK major hurricanes transition to a monotonic profile of vorticity radially inward of the RMW. Related to this monotonic profile of vorticity, WK major hurricanes possess decreased  $V_T$  at the RMW and in the outer core, and an overall flatter outer-core  $V_T$  structure at late stages in their life cycle (Fig. 14d). The structural changes are consistent with the notion that the outer-core  $V_T$  field broadens with age (Kossin et al. 2007; Musgrave et al. 2012). Inertial stability composite-mean structures stratified by TC age manifest similar changes to the vorticity profiles (not shown). These features highlight the significance of considering TC age when observing the kinematic structure of major hurricanes. The continual decrease in amplitude of the vorticity ring

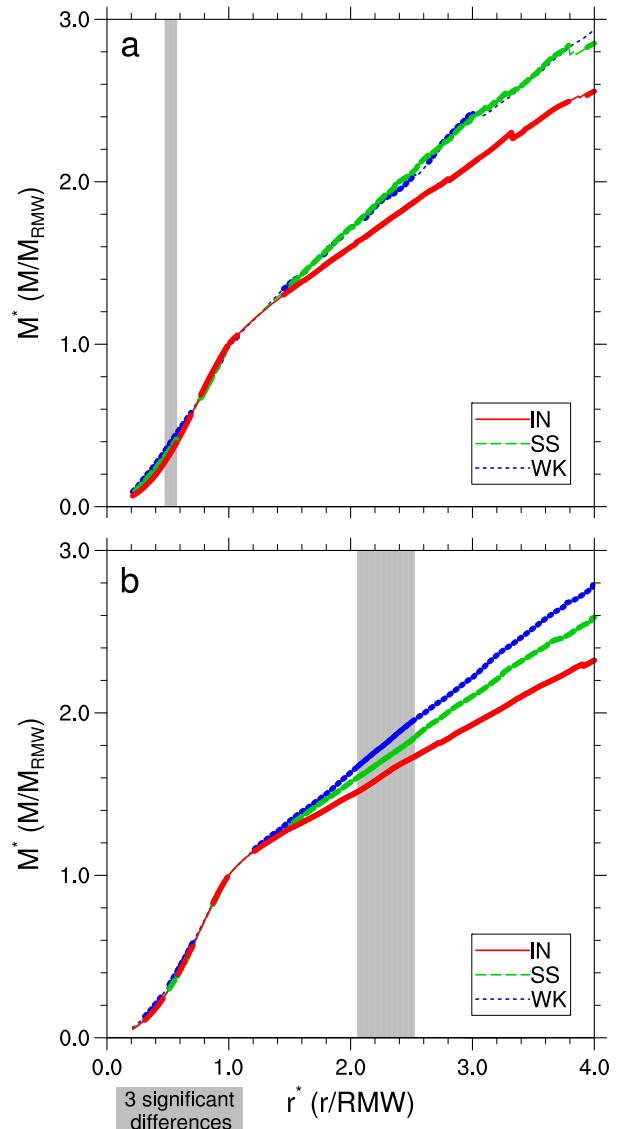


FIG. 9. As in Fig. 6, but for nondimensional absolute angular momentum.

from early stage WK major hurricanes to late stage WK major hurricanes suggests that at late stages of their life cycle, WK major hurricanes will not undergo reintensification.

In contrast to the results for major hurricanes, IN minor hurricanes have the highest outer-core vorticity compared to SS and WK minor hurricanes, along with higher inner-core vorticity associated with the vorticity ring structure (Fig. 7). Comparing the early and late stage vorticity profiles for IN minor hurricanes (cf. Figs. 15a,c) reveals that the magnitude of outer-core vorticity does not exhibit much variability with age. Instead, the outer-core vorticity of WK and SS minor hurricanes decreases during the later stages of their life

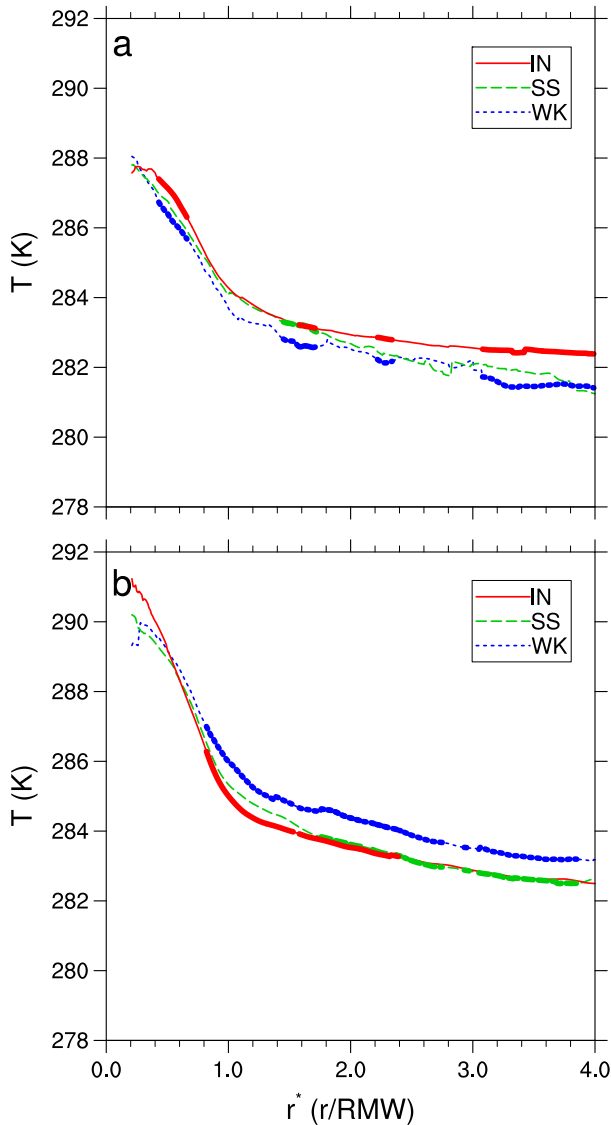


FIG. 10. As in Fig. 6, but for temperature.

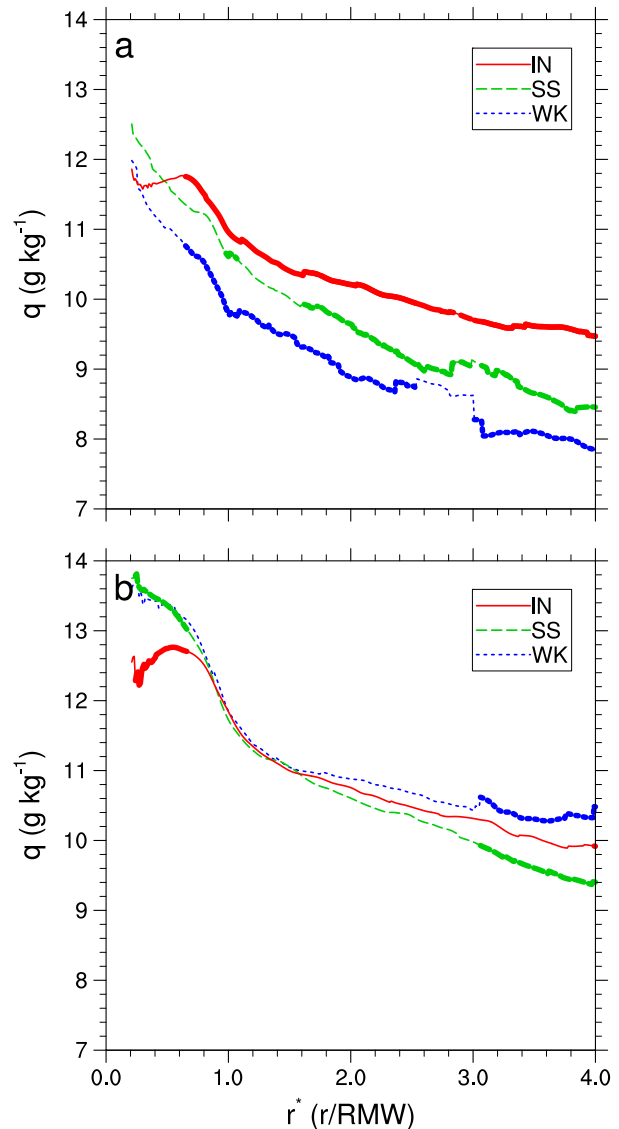


FIG. 11. As in Fig. 6, but for specific humidity.

cycles. Since WK and SS minor hurricanes are closer to the end of their life cycles (Table 4), they may have already experienced their maximum intensity and do not undergo reintensification. We speculate that convective activity in the outer-core region has diminished or weakened significantly for late stage WK and SS minor hurricanes, contributing to lower vorticity in this region. Furthermore, the results for minor hurricanes stratified by age demonstrate that the  $V_T$  structural differences in the eye primarily manifest themselves at late stages in their life cycle (Fig. 14b).

### c. Absolute angular momentum

Results for the nondimensional analysis of absolute angular momentum ( $M^*$ ) reveal that IN TCs (minor and

major hurricanes) possess the lowest absolute angular momentum at all  $r^*$  compared to SS and WK TCs. As observed in the composite-mean  $V_T$  results (Fig. 6), WK and SS major hurricanes possess a broader circulation radially outward of the RMW compared to IN major hurricanes. This broader circulation serves to increase  $M^*$  directly through higher local  $V_T$  velocities. Therefore, the WK and SS major hurricanes can possess higher outer-core  $M^*$  solely from contributions due to the TC wind field. Additionally, WK and SS TCs have higher  $M^*$  in the eye compared to IN TCs, which may be due to the effects of mixing across the eye–eyewall interface (Kossin and Eastin 2001). Therefore, the observed  $M^*$  differences at all  $r^*$  can be partially explained from contributions due to storm-scale differences.

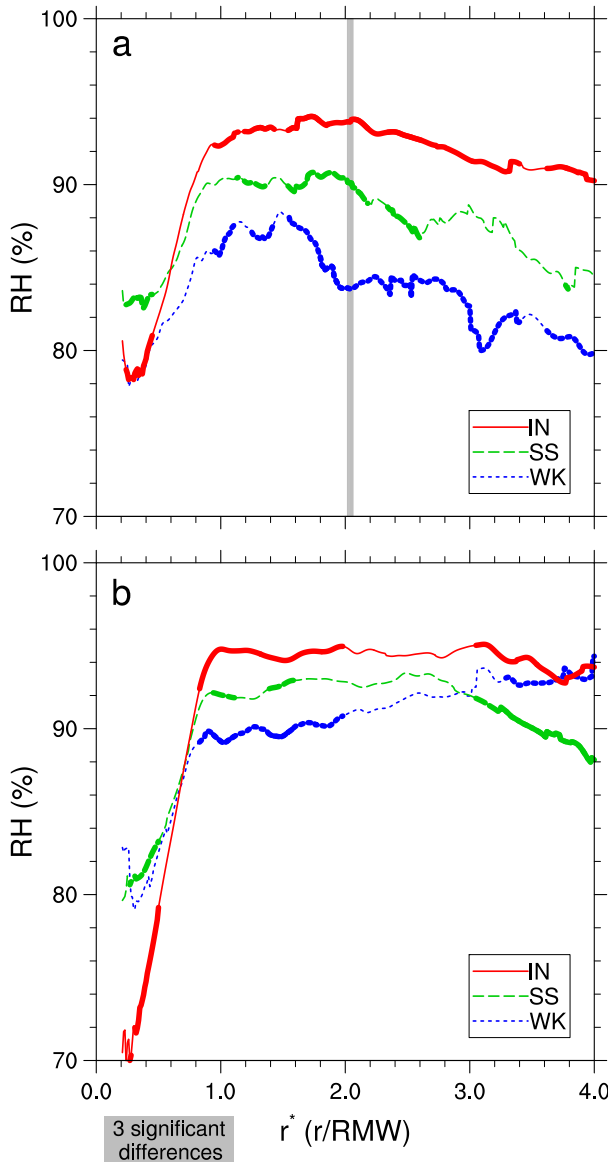


FIG. 12. As in Fig. 6, but for relative humidity.

Considering the contributions from Earth’s angular momentum, WK and SS TCs (minor and major hurricanes) are often found at higher latitudes than IN TCs. The average latitude of WK and SS TCs in this analysis is larger than IN TCs (not shown), and therefore they experience a stronger Coriolis force. We speculate that contributions from both the TC wind field and Earth’s rotation are relevant to causing lower  $M^*$  (Fig. 9) and physical absolute angular momentum (not shown) at all  $r^*$  for IN TCs. Furthermore, since  $M$  is strongly dependent on radius, the varying RMW sizes shown in Fig. 3 suggest that differences in the size of the RMW for each composite may also contribute to the observed differences in  $M^*$ .

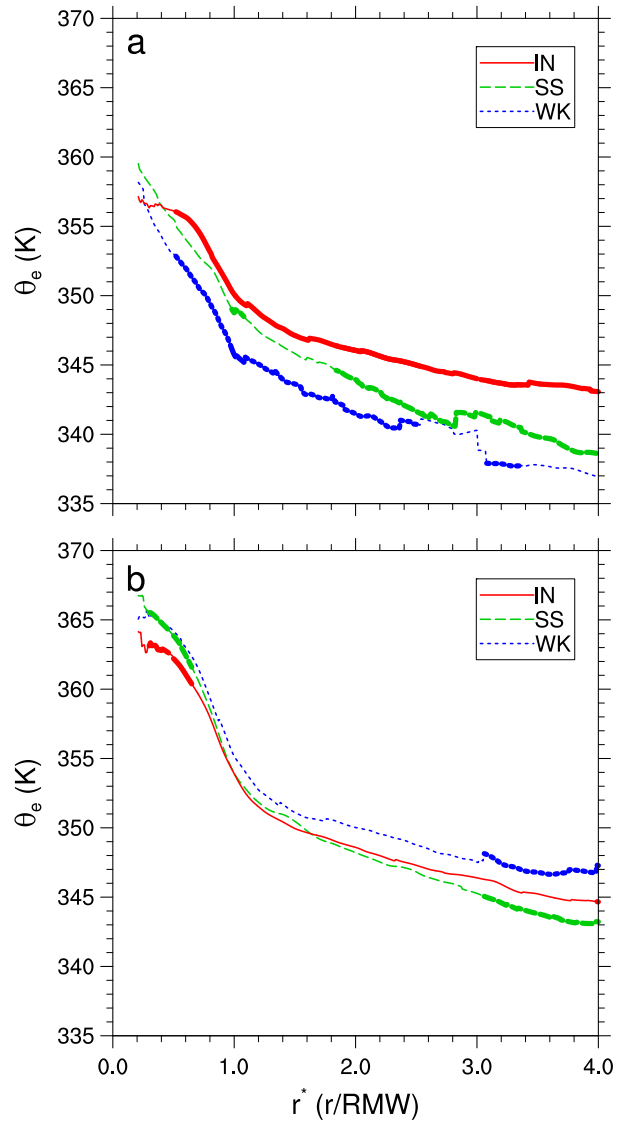


FIG. 13. As in Fig. 6, but for equivalent potential temperature.

*d. Thermodynamic structural differences*

Our results show that IN TCs (minor and major hurricanes) possess higher moisture content in the outer-core region compared to SS or WK TCs (Fig. 12). In the case of IN minor hurricanes, warmer temperatures and higher moisture (in an absolute sense) contribute to higher  $\theta_e$  relative to SS and WK minor hurricanes at nearly all  $r^*$ . Kossin and Eastin (2001) found that regime 1 (i.e., intensifying) TCs were characteristic of elevated  $\theta_e$  in the eyewall and regime 2 TCs (i.e., post-peak intensity) transitioned to a monotonic profile of  $\theta_e$ , with maximum  $\theta_e$  in the eye. Although the results for IN minor hurricanes do not necessarily indicate elevated  $\theta_e$

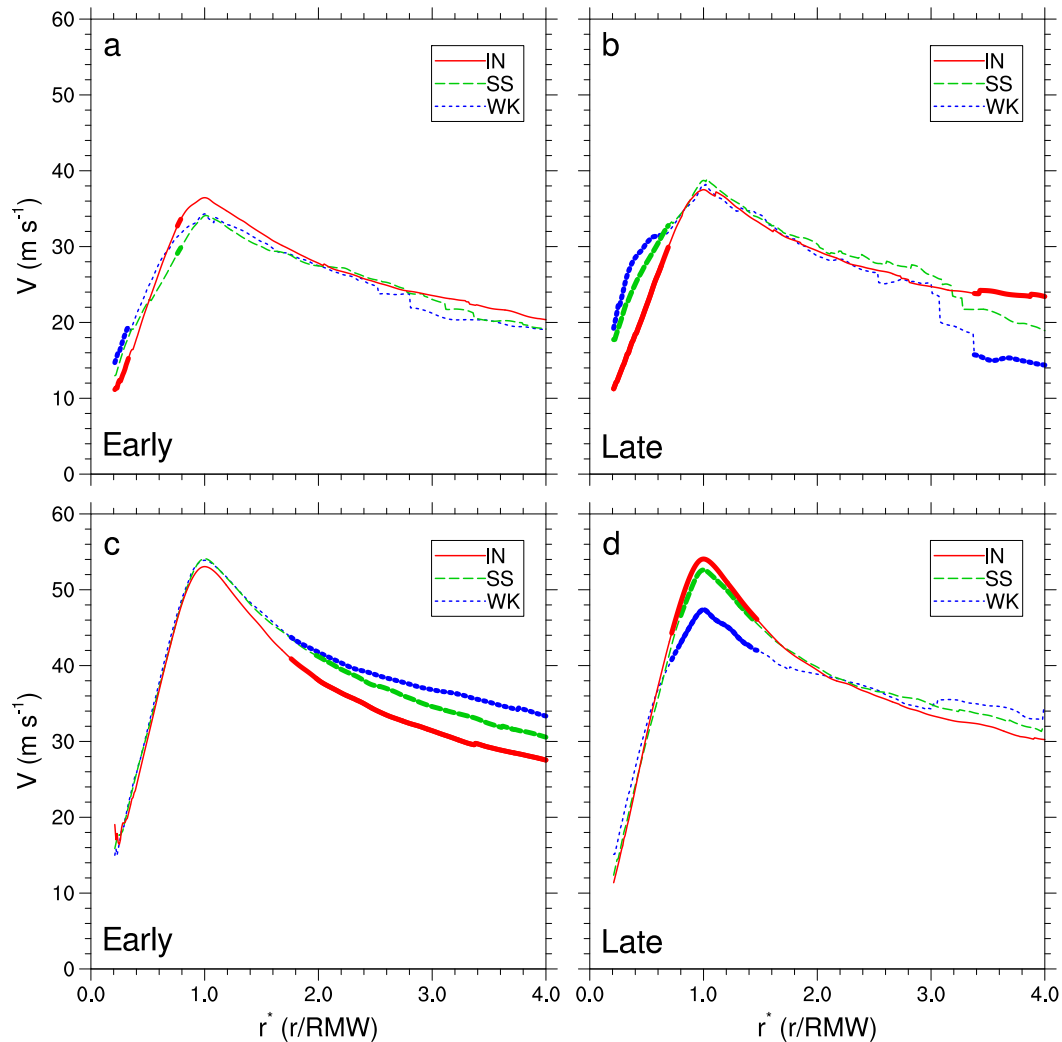


FIG. 14. Storm-relative axisymmetric tangential wind velocity composite means for (a) early stage minor hurricanes and (b) late stage minor hurricanes, and (c) early stage major hurricanes and (d) late stage major hurricanes. Intensifying (IN) TCs are denoted in solid red, steady-state (SS) TCs are denoted in dashed green, and weakening (WK) TCs are denoted in dotted blue. Radial locations where two composite means are significantly different at the 5% level appear thicker on the respective composite-mean curves.

near the eyewall, the composite has a slightly flatter  $\theta_e$  gradient in the eye than the SS and WK minor hurricanes. Higher values of  $\theta_e$  near the eyewalls of IN minor hurricanes would be consistent with the probable presence of CBs; however, thermodynamic evidence of these features is not apparent in the results presented. This does not rule out the possibility these features are present for IN minor hurricanes, but rather it suggests that the thermodynamic signal is not as strong as the kinematic signal in the azimuthally averaged composite structures. We speculate that the thermodynamic features that contribute to the different structures observed by Kossin and Eastin (2001) may evolve on time scales that are too short to be resolved after azimuthal

averaging and compositing, such as the presence of CBs, which evolve on the order of 1–3 h. Furthermore, discrepancies may arise due to pilots intentionally deviating the aircraft flight path to avoid the core of CBs for safety purposes, which would reduce the observations of elevated  $\theta_e$  that may be expected in the undiluted updraft core of a CB.

Although IN major hurricanes possess higher outer-core moisture relative to SS and WK major hurricanes (Fig. 12), the higher temperatures of WK major hurricanes result in higher  $\theta_e$  at nearly all  $r^*$ . These results contrast those presented for minor hurricanes, although the differences are only statistically significant at very large  $r^*$ . The IN major hurricanes also lack elevated  $\theta_e$

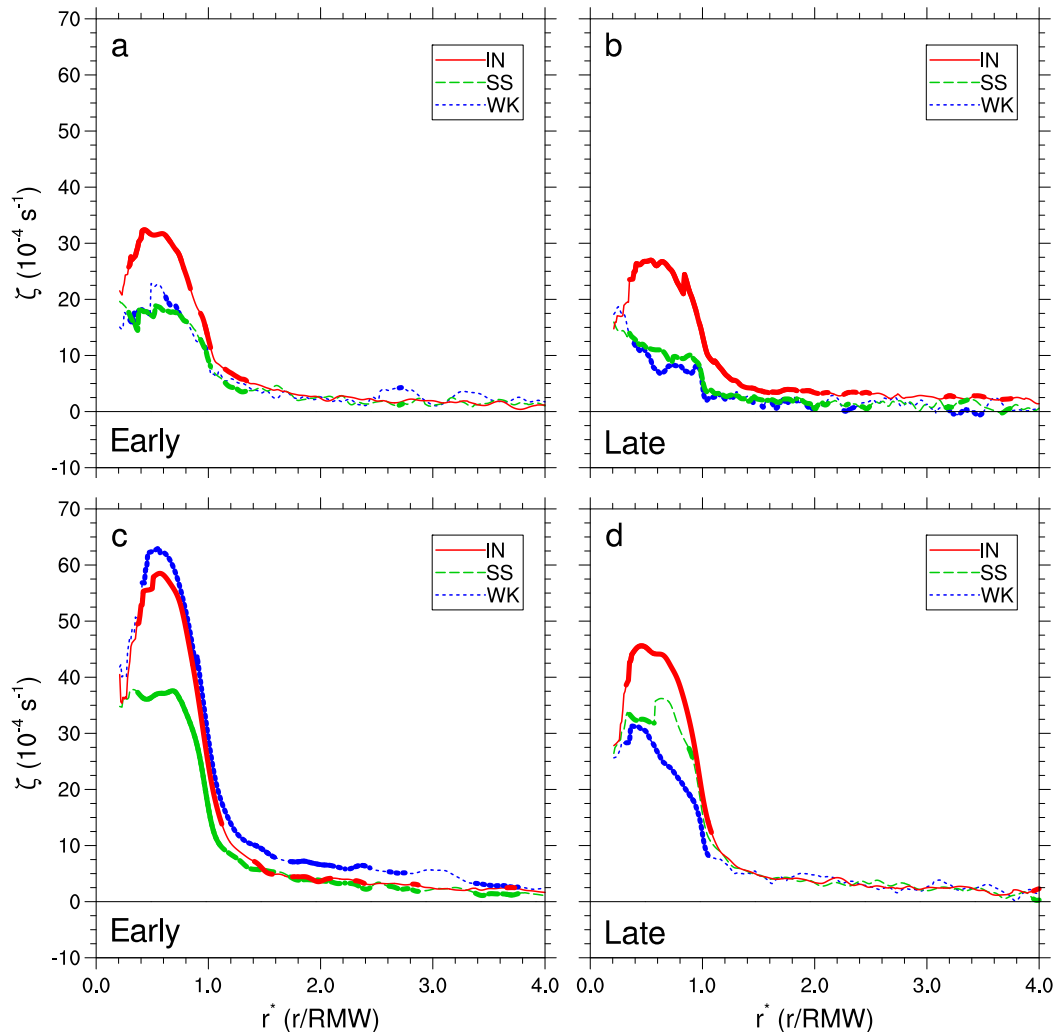


FIG. 15. As in Fig. 14, but for axisymmetric vertical vorticity.

near the eyewall, which was observed for regime 1 TCs in Kossin and Eastin (2001), similar to the IN minor hurricanes. The IN major hurricanes do, however, possess drier eyes compared to WK and SS major hurricanes, suggesting that stronger eye subsidence and adiabatic warming at 700 hPa may be key factors that distinguish IN major hurricanes from SS or WK major hurricanes. Similar results were found in earlier studies from dropsondes released into the eyes of TCs (Franklin et al. 1988; Jordan 1961). The observed moisture differences in the eye can be caused by vertical ascent and descent of the eye inversion, but they may also be caused by horizontal mixing (Willoughby 1998; Kossin and Eastin 2001). Furthermore, stronger eye subsidence may be connected to the presence of CBs within the eyewall of IN major hurricanes (Chen and Zhang 2013). Thermodynamic composites stratified by age do not reveal any new information and therefore are not shown.

#### e. Structural influences of secondary eyewalls

Formation of a secondary eyewall often leads to a broadening of the outer-core tangential wind field (Willoughby et al. 1982; Willoughby 1990; Samsury and Zipser 1995; Sitkowski et al. 2011). The presence of a secondary eyewall could have an impact on the composite-mean structures and ultimately influence the interpretation of the results. For example, if a TC was sampled during the intensification or weakening phase of an eyewall replacement cycle (ERC) [as defined by Sitkowski et al. (2011)], the outer wind maximum would contribute to higher  $V_T$  velocities, vorticity, and inertial stability in the outer-core region. On the other hand, if a TC was sampled during the reintensification phase of an ERC, the outer wind maximum would be defined as the RMW and, after normalizing the radial coordinate by the RMW, the eye, relict inner eyewall, and moat would

all be conflated (Sitkowski et al. 2011, 2012). In an effort to isolate the impacts of secondary eyewalls, each of the 233 azimuthal mean profiles included in the analysis were visually examined for the presence of a secondary wind maximum. A total of 36 cases were identified and removed from the original sample, and the composite means were recreated to examine the resulting structural differences.

Broadly speaking, the interpretation of the results remains largely unchanged, with the exception of the WK major hurricanes. Figure 16 summarizes the most notable changes after removing the secondary eyewall cases for WK major hurricanes. Figure 16a shows the smoothed azimuthal mean storm-relative tangential wind velocity and vertical vorticity sampled from a flight mission in major Hurricane Rita during the weakening phase of its ERC; a representative example of an azimuthal mean profile that was removed due to the presence of a secondary wind maximum. The primary and secondary eyewalls are apparent as local maxima in the tangential wind and vorticity, and the removal of similar cases from the WK major hurricane bin results in an overall decrease of vorticity at all  $r^*$  (cf. Figs. 7b, 16b). There is a relatively large decrease in the amplitude of the primary vorticity ring after the removal of secondary eyewall cases, which is believed to be due to the fact that TCs are near peak intensity at the beginning of the weakening phase. Since the majority (7 out of 9) of the secondary eyewall cases removed from the WK major hurricane bin exhibit a similar structure to that shown for Rita (i.e., end of the intensification or beginning of the weakening phase of an ERC), the resulting composite-mean vorticity structure has a weaker vorticity ring. The removal of the secondary eyewall cases from the WK major hurricane bin also removes statistically significant differences in the outer-core  $V_T$  between IN and WK major hurricanes (i.e., the entire WK major hurricane composite-mean structure possesses weaker  $V_T$ ). The WK major hurricanes still possess the slowest decay of  $V_T$  radially outward of the RMW compared to IN and SS major hurricanes (not shown), but the statistically significant differences in outer-core vorticity are also removed. Other minor numerical differences were noted in the other composite-mean profiles, but the physical interpretation of the structures described herein remains unchanged.

## 6. Summary and conclusions

In situ data obtained from the FLIGHT+ dataset (Vigh et al. 2016) were used to investigate the 700-hPa kinematic and thermodynamic structure of North Atlantic basin TCs stratified by intensity, intensity change,

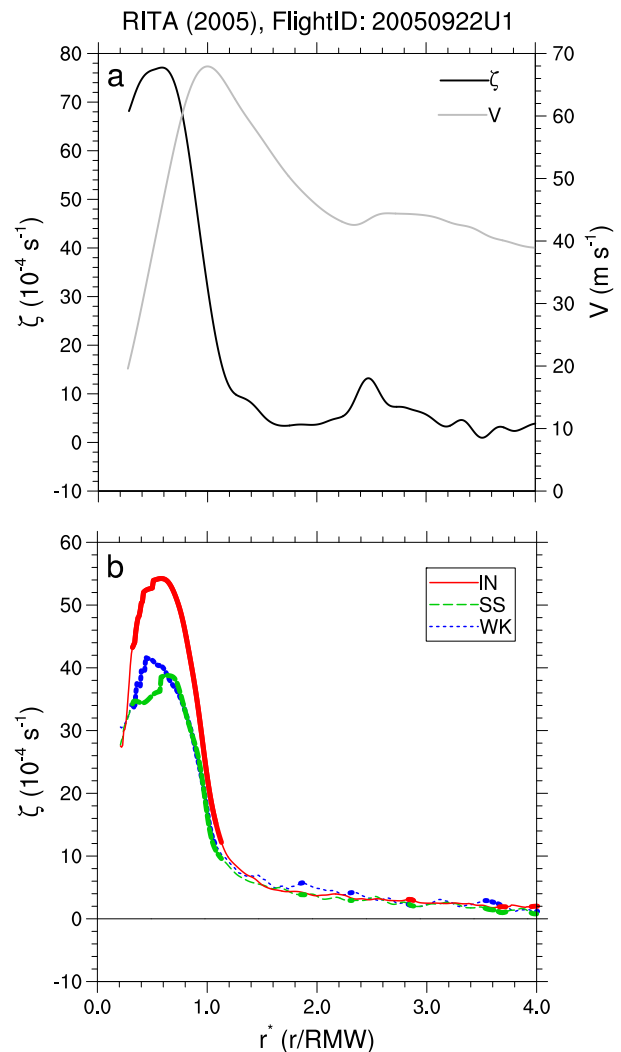


FIG. 16. (a) Smoothed azimuthal mean storm-relative tangential wind velocity and vertical vorticity sampled in Hurricane Rita during the weakening phase of its ERC. (b) Composite means of axisymmetric vertical vorticity for major hurricanes (as in Fig. 7b), after the removal of secondary eyewall cases.

and age from 1999 to 2012. Composite-mean structures were created for “minor” hurricanes ( $64 \leq v_{\max} < 96$  kt) and “major” hurricanes ( $v_{\max} \geq 96$  kt) according to the Saffir–Simpson hurricane wind scale that were weakening (WK), steady state (SS), or intensifying (IN). The results of this study are broadly consistent with previous studies that investigated structure with respect to intensity (Mallen et al. 2005; Pendergrass and Willoughby 2009; Shapiro and Willoughby 1982; Vigh and Schubert 2009) or intensity change (Kossin and Eastin 2001; Rogers et al. 2013, 2015), but the larger sample size allows for a multivariate stratification that indicates some structural features depend on both of these factors. Furthermore, the results suggest that the TC age can be

used to distinguish structural differences. Prior observational studies have speculated toward the potential influence of secondary eyewalls on their composite structures (Mallen et al. 2005; Rogers et al. 2013), but did not remove those cases and were unable to make a definitive statement on the resulting changes. Here we demonstrate that the influence of secondary eyewalls primarily manifests themselves in the inner and outer core of WK major hurricanes, but that the primary results of this study remain largely unchanged after removal of these cases. The main findings reported in this study can be summarized as follows:

- Kinematically, IN TCs can be distinguished from WK or SS TCs by steep tangential wind gradients, a vorticity ring structure found radially inward of the radius of maximum tangential wind (RMW), higher inertial stability radially inward of the RMW, and lower nondimensional absolute angular momentum at all normalized radii.
- The IN TCs are distinguished from SS or WK TCs by higher moisture content, as measured by both specific and relative humidity, in the inner- and outer-core regions. Furthermore, IN major hurricanes possess drier eyes compared to SS and WK major hurricanes. The IN minor hurricanes possess the highest  $\theta_e$  at all normalized radii compared to SS or WK minor hurricanes, although no significant pattern distinguishing major hurricanes is found for  $\theta_e$ .
- While a vorticity ring is a distinguishing feature for IN minor hurricanes, this distinction is reduced in major hurricanes that have a pronounced vorticity ring for both the IN and WK composite means. The results suggest that the eventual decay of the vorticity ring for WK major hurricanes may occur from the effects of either a secondary eyewall or radial mixing at the eye–eyewall interface. The SS TCs tend to have a nearly flat and close to monotonic vorticity profile regardless of their intensity.
- Additional stratification of the results by TC age reveal that the tangential wind structural differences found in the eye of minor hurricanes manifest themselves more significantly at late stages in their life cycle. The combination of stronger tangential winds and a monopolar vorticity structure in the eye of late stage SS and WK minor hurricanes supports the transition toward solid-body rotation resulting from eye–eyewall mixing processes (Kossin and Eastin 2001; Schubert et al. 1999). The tangential wind structural differences in the outer core of major hurricanes are primarily observed during early stages of their life cycle and can be explained in part by the presence of secondary eyewalls.

The main composite-mean structural differences summarized here are statistically significant at the 5% level, providing further evidence that these features represent distinguishing factors that may be of benefit for TC intensity forecasting. The primary focus of this study has been on discussion of structural differences that are largely influenced by internal processes, although external environmental influences can also play an important role. Martinez (2016) demonstrated that for the same composites presented in this study, minor hurricanes had more statistically significant differences in their large scale environments compared to major hurricanes which are generally found in favorable environments (see their Table 5.2). The variability in major hurricane structure shown in the current study is consistent with the notion that TC intensification rates are primarily controlled by internal processes given a favorable preexisting environment (Hendricks et al. 2010). Some of the structural differences in the minor hurricanes may be reflective of the influence of large-scale environments, but the current results provide new information about the common internal structures across the intensity change spectrum. Many of the structural differences presented in this study are intuitive and can be applied subjectively for forecasting (e.g., higher moisture in the inner core is more favorable for intensification), but the composite statistics presented here can also provide a framework for quantitative, objective forecasting improvements based on aircraft measurements in a manner similar to statistical-dynamical models that use environmental information as predictors (DeMaria et al. 2005; Kaplan et al. 2010). Future work will investigate the shapes of the tangential wind profiles for each of the composites presented in this study at various radial segments to identify significant differences, for example, between intensifying and weakening TCs. This information could complement previous work aimed at developing parametric wind profiles of TCs, which are often used in storm-surge, wind risk, and catastrophe forecasting models (Willoughby et al. 2006; Holland et al. 2010).

Although the composite approach taken in this study has identified significant structural differences, we can only speculate on the main physical processes that contribute to the observed structural differences. Additional work must be carried out to further identify the key physical processes that distinguish these groups of TCs. The research presented could be complemented by case studies examining the physical processes occurring in WK, SS, and IN minor and major hurricanes. Furthermore, high-resolution numerical simulations could also augment our findings by providing temporal resolution that is often not

available with observations. Detailed field observations gathered throughout the full depth of the troposphere will be examined to gain insight in regards to the main physical processes occurring as a TC intensifies, weakens, or remains steady state. These observations may provide key information to further elucidate the results presented in this study.

*Acknowledgments.* This study was supported by the National Science Foundation (NSF) CAREER Award AGS-1349881 and Office of Naval Research Award N000141410118. JM was supported, in part, by the Significant Opportunities in Atmospheric Research and Science (SOARS) Program, NSF Grant AGS-1120459 and the National Science Foundation Bridge to the Doctorate Fellowship, NSF Grant 004863-00003. We thank the crews of both the 53rd Weather Reconnaissance Squadron and NOAA Aircraft Operations Center whose hours of hard work and dedication to collecting high-quality observations in tropical cyclones made this research possible. We would also like to thank Gary Barnes, Yuqing Wang, Jim Kossin, and two anonymous reviewers for their insightful comments that improved the quality of the manuscript. The Extended Flight Level Dataset (FLIGHT+) for tropical cyclones was created by the Research Applications Laboratory at the National Center for Atmospheric Research (NCAR) from data provided by the NOAA Hurricane Research Division of AOML and U.S. Air Force Reserve. The National Center for Atmospheric Research is sponsored by the National Science Foundation. The creation of this dataset was funded through a grant from the Bermuda Institute of Ocean Sciences Risk Prediction Initiative (RPI2.0). We especially thank Neal Dorst (AOML/HRD) for creating the wind center tracks and assembling the data and metadata that were vital for creation of the FLIGHT+ dataset.

#### REFERENCES

- Barnes, G. M., J. F. Gamache, M. A. LeMone, and G. J. Stossmeister, 1991: A convective cell in a hurricane rainband. *Mon. Wea. Rev.*, **119**, 776–794, doi:10.1175/1520-0493(1991)119<0776:ACCIAH>2.0.CO;2.
- Bolton, D., 1980: The computation of equivalent potential temperature. *Mon. Wea. Rev.*, **108**, 1046–1053, doi:10.1175/1520-0493(1980)108<1046:TCOEPT>2.0.CO;2.
- Chen, H., and D.-L. Zhang, 2013: On the rapid intensification of Hurricane Wilma (2005). Part II: Convective bursts and the upper-level warm core. *J. Atmos. Sci.*, **70**, 146–162, doi:10.1175/JAS-D-12-062.1.
- DeMaria, M., M. Mainelli, L. K. Shay, J. A. Knaff, and J. Kaplan, 2005: Further improvements to the Statistical Hurricane Intensity Prediction Scheme (SHIPS). *Wea. Forecasting*, **20**, 531–543, doi:10.1175/WAF862.1.
- , C. R. Sampson, J. A. Knaff, and K. D. Musgrave, 2014: Is tropical cyclone intensity guidance improving? *Bull. Amer. Meteor. Soc.*, **95**, 387–398, doi:10.1175/BAMS-D-12-00240.1.
- Duchon, C. E., 1979: Lanczos filtering in one and two dimensions. *J. Appl. Meteor.*, **18**, 1016–1022, doi:10.1175/1520-0450(1979)018<1016:LFIOAT>2.0.CO;2.
- Eastin, M. D., P. G. Black, and W. M. Gray, 2002: Flight level thermodynamic instrument wetting errors in hurricanes. Part I: Observations. *Mon. Wea. Rev.*, **130**, 825–841, doi:10.1175/1520-0493(2002)130<0825:FLTIWE>2.0.CO;2.
- Franklin, J. L., S. J. Lord, and F. D. Marks Jr., 1988: Dropwindsonde and radar observations of the eye of Hurricane Gloria (1985). *Mon. Wea. Rev.*, **116**, 1237–1244, doi:10.1175/1520-0493(1988)116<1237:DAROOT>2.0.CO;2.
- Hendricks, E. A., W. H. Schubert, R. K. Taft, H. Wang, and J. P. Kossin, 2009: Life cycles of hurricane-like vorticity rings. *J. Atmos. Sci.*, **66**, 705–722, doi:10.1175/2008JAS2820.1.
- , M. S. Peng, B. Fu, and T. Li, 2010: Quantifying environmental control on tropical cyclone intensity change. *Mon. Wea. Rev.*, **138**, 3243–3271, doi:10.1175/2010MWR3185.1.
- , B. D. McNoldy, and W. H. Schubert, 2012: Observed inner-core structural variability in Hurricane Dolly (2008). *Mon. Wea. Rev.*, **140**, 4066–4077, doi:10.1175/MWR-D-12-00018.1.
- , W. H. Schubert, Y.-H. Chen, H.-C. Kuo, and M. S. Peng, 2014: Hurricane eyewall evolution in a forced shallow-water model. *J. Atmos. Sci.*, **71**, 1623–1643, doi:10.1175/JAS-D-13-0303.1.
- Holland, G. J., J. I. Belanger, and A. Fritz, 2010: A revised model for radial profiles of hurricane winds. *Mon. Wea. Rev.*, **138**, 4393–4401, doi:10.1175/2010MWR3317.1.
- Jarvinen, B. R., C. J. Neumann, and M. A. S. Davis, 1984: A tropical cyclone data tape for the North Atlantic Basin, 1886–1983: Contents, limitations, and uses. NOAA Tech. Memo. NWS NHC 22, Coral Gables, FL, 24 pp., <http://www.nhc.noaa.gov/pdf/NWS-NHC-1988-22.pdf>.
- Jordan, C. L., 1961: Marked changes in the characteristics of the eye of intense typhoons between the deepening and filling stages. *J. Meteor.*, **18**, 779–789, doi:10.1175/1520-0469(1961)018<0779:MCITCO>2.0.CO;2.
- Kaplan, J., M. DeMaria, and J. A. Knaff, 2010: A revised tropical cyclone rapid intensification index for the North Atlantic and eastern North Pacific basins. *Wea. Forecasting*, **25**, 220–241, doi:10.1175/2009WAF2222280.1.
- Knaff, J. A., J. P. Kossin, and M. DeMaria, 2003: Annular hurricanes. *Wea. Forecasting*, **18**, 204–223, doi:10.1175/1520-0434(2003)018<0204:AH>2.0.CO;2.
- Kossin, J. P., and M. D. Eastin, 2001: Two distinct regimes in the kinematic and thermodynamic structure of the hurricane eye and eyewall. *J. Atmos. Sci.*, **58**, 1079–1090, doi:10.1175/1520-0469(2001)058<1079:TDRITK>2.0.CO;2.
- , and W. H. Schubert, 2001: Mesovortices, polygonal flow patterns, and rapid pressure falls in hurricane-like vortices. *J. Atmos. Sci.*, **58**, 2196–2209, doi:10.1175/1520-0469(2001)058<2196:MPFPAR>2.0.CO;2.
- , J. A. Knaff, H. I. Berger, D. C. Herndon, T. A. Cram, C. S. Velden, R. J. Murnane, and J. D. Hawkins, 2007: Estimating hurricane wind structure in the absence of aircraft reconnaissance. *Wea. Forecasting*, **22**, 89–101, doi:10.1175/WAF985.1.
- Landsea, C. W., and J. L. Franklin, 2013: Atlantic hurricane database uncertainty and presentation of a new database format. *Mon. Wea. Rev.*, **141**, 3576–3592, doi:10.1175/MWR-D-12-00254.1.

- Lee, W.-C., and M. M. Bell, 2007: Rapid intensification, eyewall contraction, and breakdown of Hurricane Charley (2004) near landfall. *Geophys. Res. Lett.*, **34**, L02802, doi:10.1029/2006GL027889.
- Mallen, K. J., M. T. Montgomery, and B. Wang, 2005: Reexamining the near-core radial structure of the tropical cyclone primary circulation: Implications for vortex resiliency. *J. Atmos. Sci.*, **62**, 408–425, doi:10.1175/JAS-3377.1.
- Martinez, J., 2016: Examination of tropical cyclone structure and intensification with the Extended Flight Level Dataset (FLIGHT+) from 1999 to 2012. M.S. thesis, Department of Atmospheric Science, University of Hawai'i at Mānoa, 67 pp.
- McAdie, C. J., C. W. Landsea, C. J. Neumann, J. E. David, and E. S. Blake, 2009: *Tropical Cyclones of the North Atlantic Ocean, 1851–2006*. Historical Climatology Series, No. 6-2, National Climatic Data Center, 238 pp.
- Musgrave, K. D., R. K. Taft, J. L. Vigh, B. D. McNoldy, and W. H. Schubert, 2012: Time evolution of the intensity and size of tropical cyclones. *J. Adv. Model. Earth Syst.*, **4**, M08001, doi:10.1029/2011MS000104.
- Pendergrass, A. G., and H. E. Willoughby, 2009: Diabatically induced secondary flows in tropical cyclones. Part I: Quasi-steady forcing. *Mon. Wea. Rev.*, **137**, 805–821, doi:10.1175/2008MWR2657.1.
- Rogers, R., 2010: Convective-scale structure and evolution during a high-resolution simulation of tropical cyclone rapid intensification. *J. Atmos. Sci.*, **67**, 44–70, doi:10.1175/2009JAS3122.1.
- , P. Reasor, and S. Lorsolo, 2013: Airborne Doppler observations of the inner-core structural differences between intensifying and steady state tropical cyclones. *Mon. Wea. Rev.*, **141**, 2970–2991, doi:10.1175/MWR-D-12-00357.1.
- , —, and J. A. Zhang, 2015: Multiscale structure and evolution of Hurricane Earl (2010) during rapid intensification. *Mon. Wea. Rev.*, **143**, 536–562, doi:10.1175/MWR-D-14-00175.1.
- Rozoff, C. M., J. P. Kossin, W. H. Schubert, and P. J. Mulero, 2009: Internal control of hurricane intensity variability: The dual nature of potential vorticity mixing. *J. Atmos. Sci.*, **66**, 133–147, doi:10.1175/2008JAS2717.1.
- Samsury, C. E., and E. J. Zipser, 1995: Secondary wind maxima in hurricanes: Airflow and relationship to rainbands. *Mon. Wea. Rev.*, **123**, 3502–3517, doi:10.1175/1520-0493(1995)123<3502:SWMIHA>2.0.CO;2.
- Schubert, W. H., and J. J. Hack, 1982: Inertial stability and tropical cyclone development. *J. Atmos. Sci.*, **39**, 1687–1697, doi:10.1175/1520-0469(1982)039<1687:ISATCD>2.0.CO;2.
- , M. T. Montgomery, R. K. Taft, T. A. Guinn, S. R. Fulton, J. P. Kossin, and J. P. Edwards, 1999: Polygonal eyewalls, asymmetric eye contraction, and potential vorticity mixing in hurricanes. *J. Atmos. Sci.*, **56**, 1197–1223, doi:10.1175/1520-0469(1999)056<1197:PEAECA>2.0.CO;2.
- Shapiro, L. J., and H. E. Willoughby, 1982: The response of balanced hurricanes to local sources of heat and momentum. *J. Atmos. Sci.*, **39**, 378–394, doi:10.1175/1520-0469(1982)039<0378:TROBHT>2.0.CO;2.
- Shea, D. J., and W. M. Gray, 1973: The hurricane's inner core region. I. Symmetric and asymmetric structure. *J. Atmos. Sci.*, **30**, 1544–1564, doi:10.1175/1520-0469(1973)030<1544:THICRI>2.0.CO;2.
- Sitkowski, M., J. P. Kossin, and C. M. Rozoff, 2011: Intensity and structure changes during hurricane eyewall replacement cycles. *Mon. Wea. Rev.*, **139**, 3829–3847, doi:10.1175/MWR-D-11-00034.1.
- , —, —, and J. A. Knaff, 2012: Hurricane eyewall replacement cycle thermodynamics and the relict inner eyewall circulation. *Mon. Wea. Rev.*, **140**, 4035–4045, doi:10.1175/MWR-D-11-00349.1.
- Smith, R. K., and M. T. Montgomery, 2016: The efficiency of diabatic heating and tropical cyclone intensification. *Quart. J. Roy. Meteor. Soc.*, **142**, 2081–2086, doi:10.1002/qj.2804.
- , —, and N. V. Sang, 2009: Tropical cyclone spin-up revisited. *Quart. J. Roy. Meteor. Soc.*, **135**, 1321–1335, doi:10.1002/qj.428.
- Vigh, J. L., and W. H. Schubert, 2009: Rapid development of the tropical cyclone warm core. *J. Atmos. Sci.*, **66**, 3335–3350, doi:10.1175/2009JAS3092.1.
- , and Coauthors, 2016: FLIGHT+: The Extended Flight Level Dataset for Tropical Cyclones (version 1.1). Tropical Cyclone Data Project, National Center for Atmospheric Research, Research Applications Laboratory, Boulder, CO, accessed 31 May 2016, doi:10.5065/D6WS8R93.
- Willoughby, H. E., 1990: Temporal changes of the primary circulation in tropical cyclones. *J. Atmos. Sci.*, **47**, 242–264, doi:10.1175/1520-0469(1990)047<0242:TCOTPC>2.0.CO;2.
- , 1998: Tropical cyclone eye thermodynamics. *Mon. Wea. Rev.*, **126**, 3053–3067, doi:10.1175/1520-0493(1998)126<3053:TCET>2.0.CO;2.
- , and M. B. Chelmw, 1982: Objective determination of hurricane tracks from aircraft observations. *Mon. Wea. Rev.*, **110**, 1298–1305, doi:10.1175/1520-0493(1982)110<1298:ODOHTF>2.0.CO;2.
- , J. A. Clos, and M. G. Shoreibah, 1982: Concentric eye walls, secondary wind maxima, and evolution of the hurricane vortex. *J. Atmos. Sci.*, **39**, 395–411, doi:10.1175/1520-0469(1982)039<0395:CEWSWM>2.0.CO;2.
- , R. W. R. Darling, and M. E. Rahn, 2006: Parametric representation of the primary hurricane vortex. Part II: A new family of sectionally continuous profiles. *Mon. Wea. Rev.*, **134**, 1102–1120, doi:10.1175/MWR3106.1.
- Zipser, E. J., R. J. Meitin, and M. A. LeMone, 1981: Mesoscale motion fields associated with slowly moving gate convective band. *J. Atmos. Sci.*, **38**, 1725–1750, doi:10.1175/1520-0469(1981)038<1725:MMFAWA>2.0.CO;2.